

Fermi Bubbles in the Milky Way: the closest AGN feedback laboratory courtesy of Sgr A*?

Kastytis Zubovas* and Sergei Nayakshin

Dept. of Physics & Astronomy, University of Leicester, Leicester, LE1 7RH, UK

14 November 2018

ABSTRACT

Deposition of a massive (10^4 to $10^5 M_\odot$) giant molecular cloud (GMC) into the inner parsec of the Galaxy is widely believed to explain the origin of over a hundred unusually massive young stars born there ~ 6 Myr ago. An unknown fraction of that gas could have been accreted by Sgr A*, the supermassive black hole (SMBH) of the Milky Way. It has been recently suggested that two observed γ -ray-emitting bubbles emanating from the very center of our Galaxy were inflated by this putative activity of Sgr A*. We run a suite of numerical simulations to test whether the observed morphology of the bubbles could be due to the collimation of a wide angle outflow from Sgr A* by the disc-like Central Molecular Zone (CMZ), a well known massive repository of molecular gas in the central ~ 200 pc. We find that an Eddington-limited outburst of Sgr A* lasting $\simeq 1$ Myr is required to reproduce the morphology of the *Fermi* bubbles, suggesting that the GMC mass was $\sim 10^5 M_\odot$ and it was mainly accreted by Sgr A* rather than used to make stars. We also find that the outflow from Sgr A* enforces strong angular momentum mixing in the CMZ disc, robustly sculpting it into a much narrower structure – a ring – perhaps synonymous with the recently reported “*Herschel* ring”. In addition, we find that Sgr A* outflow is likely to have induced formation of massive star-forming GMCs in the CMZ. In this scenario, the Arches and Quintuplet clusters, the two observed young star clusters in the central tens of parsecs of the Galaxy, and also GMCs such as Sgr B2, owe their existence to the recent Sgr A* activity.

Key words: galaxies:evolution - galaxies:individual:Milky Way - quasars:general - black hole physics - accretion

1 INTRODUCTION

The Galactic centre (GC) is a particularly interesting astrophysical location, primarily due to the presence of the closest supermassive black hole (SMBH) - Sgr A*, whose mass is $M_{\text{bh}} \simeq 4 \times 10^6 M_\odot$ (Schödel et al. 2002; Ghez et al. 2005, 2008). Although the Soltan relation (Soltan 1982) implies that Sgr A* gained most of its mass through luminous accretion, it is currently very dim in comparison with active galactic nuclei (AGN): its X-ray luminosity is less than $\sim 10^{-11} L_{\text{Edd}}$ (where $L_{\text{Edd}} \sim$ a few $\times 10^{44}$ erg s^{-1} is its Eddington luminosity; Baganoff et al. 2003). Sgr A* dimness has stimulated development of radiatively inefficient accretion and accretion/outflow solutions (e.g., Narayan et al. 1995; Blandford & Begelman 1999). However, X-ray reflection nebulae suggest that Sgr A* might have been much brighter about a hundred years ago, with luminosity of a

few $\times 10^{39}$ erg s^{-1} in X-rays (e.g. Revnivtsev et al. 2004; Ponti et al. 2010). This variability may reflect feeding events from a few pc-scale molecular gas reservoirs (Morris et al. 1999) or variability in the wind capture rate from the young massive stars near Sgr A* that feed it presently (Cuadra et al. 2008).

A recent observation may shed a rather unexpected light on a much earlier but still rather recent activity of Sgr A*. *Fermi*-LAT data has been recently analysed to reveal two giant γ -ray emitting bubbles, disposed symmetrically on either side of the Galactic plane (Su et al. 2010; although see Dobler et al. 2011 for a different interpretation). They are roughly teardrop-shaped and extend $\sim 8 - 10$ kpc above and below the plane, but are centred on Sgr A* with a narrow ($d \sim 100$ pc) waist along the plane. The limbs of the lobes coincide with the extended structure seen in medium-energy X-rays by ROSAT (Snowden et al. 1997). The lobes have γ -ray luminosity $L_\gamma \simeq 4 \times 10^{37}$ erg s^{-1} . Observational constraints (Su et al. 2010) and emission mod-

* E-mail: kastytis.zubovas@astro.le.ac.uk

elling (Crocker & Aharonian 2011) allows one to estimate the total kinetic and thermal energy content of the *Fermi* bubbles as $E_{\text{bub}} \sim 10^{54-55}$ erg.

There has been a number of suggestions as to what the origin of the *Fermi* bubbles might be. Su et al. (2010) discuss several physical processes and provide a constraint that if the bubbles are older than a few $\times 10^6$ yr, the γ -ray emission must be powered by ions rather than electrons due to a short cooling time of the latter (see their section 7.1 and Figure 28), unless electrons are continuously accelerated within the bubbles (which may not be unreasonable; see §5.4 below). Crocker et al. (2011) and Crocker & Aharonian (2011) detailed these arguments further and suggested that the emission is powered by cosmic ray (CR) protons rather than electrons. They further consider a quasi-steady state model in which the CR protons are continuously injected by supernova explosions. CR protons and heavier ions are then trapped inside the bubbles for the lifetime of the latter (which the authors require to be about 10 Gyrs). On the other hand, Mertsch & Sarkar (2011) argued that the emission spectrum of the bubbles is inconsistent with CR protons and therefore the bubbles must be a recent, cosmic ray electron-powered, feature.

The scenario with a more recent origin of the bubbles has been investigated by several authors. Guo & Mathews (2011) suggest that a jet launched by Sgr A* 1 – 2 Myr ago could create the morphology and emission structure observed. Cheng et al. (2011) argue that the bubbles are inflated by episodic Sgr A* activity caused by tidal disruptions of stars passing too close to Sgr A*. Zubovas et al. (2011, hereafter Paper I) argue that an almost spherical outflow from Sgr A* caused by a short burst of AGN activity coincident with the well-known star formation (SF) event 6 Myr ago (Paumard et al. 2006), can be the origin of the bubbles. In the model, the outflow from Sgr A* is suggested to be quasi-spherical at launch as is required to explain the observed $M_{\text{bh}} - \sigma$ relations for classical bulges and elliptical galaxies (King 2003, 2005, 2010a). The outflow becomes collimated by interaction with a disc-like structure, the Central Molecular Zone - a dense ring (aspect ratio $H/R \sim 0.2-0.3$) of predominantly molecular gas extending from the Galaxy centre to ~ 200 pc. This collimation explains the large width of the bubbles and their symmetry with respect to the Galactic plane, which is not at all guaranteed by a jet model, since jet directions are known to be completely uncorrelated with the large-scale structure of the host galaxies (Kinney et al. 2000; Nagar & Wilson 1999). Zubovas et al. (2011) estimated the duration of the quasar phase to be at the minimum $t_q = 5 \times 10^4$ yr and the mass of gas accreted by Sgr A*, $\Delta M > 4 \times 10^3 M_{\odot}$, comparable to the mass in the young stars in the central parsec, $M_* \sim \text{few to ten } \times 10^3 M_{\odot}$ (Paumard et al. 2006).

In this paper, we test the analytical results of Paper I by performing numerical simulations. We broadly follow the methodology of simulating spherical outflows from accreting SMBHs of Nayakshin & Power (2010). These SPH simulations involve a prescription for passing momentum and energy of the outflow to the ambient gas (Nayakshin et al. 2009). The method has been shown (Nayakshin & Power 2010) to reproduce the analytical results of the wind feedback model we use here (King 2003). We aim to investigate whether the morphology, size and energy content of the bub-

bles can be reproduced with this model. In addition, we are interested in constraints that the simulations could place on a key unknown of the problem – the duration of Sgr A* activity. We find that a longer quasar outburst is needed than found in Paper I, most likely because the energy produced by Sgr A* outflow is spread more widely in the simulations, e.g., outside the bubbles themselves, than assumed analytically.

The Paper is structured as follows. In Section 2, we review our analytical model and the main results of Paper I. In Section 3, we describe the numerical model and the initial conditions of the simulations. We follow this by presenting the results in Section 4 and discussing their implications in Section 5. We briefly summarize and conclude in Section 6.

2 A PHYSICAL MODEL FOR THE *FERMI* BUBBLES

2.1 Sgr A* as the power source

As explained in Paper I, our Sgr A* feedback model is based on the analytical models of fast wind outflows from supermassive black holes by King (2003, 2005, 2010b,a), tailored to the present day inner Milky Way. Here we summarise the key assumptions behind this model.

Fast ($v \sim 0.1c$) wide-angle outflows from AGN have been revealed by observations of blue-shifted X-ray absorption lines; they appear to be a ubiquitous feature, detected in $\sim 40\%$ of AGN (Tombesi et al. 2010a,b). Recent XMM observations (Pounds & Vaughan 2011) of X-ray emission from a limb-brightened shell of post-shock gas building up ahead of the contact discontinuity corroborate these results and the model of King (2003) further. The outflows are probably driven by radiation pressure of photons emitted by Sgr A* on the gas in the innermost regions of black hole accretion flows. While some anisotropy in the outflow may be present in general, here we consider a spherical outflow for simplicity and demonstrate that it is the properties of the host galaxy that may mold the outflows into the teardrop-like shape.

We assume that Sgr A* accretion rate is mildly super-Eddington, and that its luminosity is limited by the Eddington limit. We do not model the sub-parsec scale disc(s) from which Sgr A* would be accreting gas here. As shown by Nayakshin & Cuadra (2005) and Alexander et al. (2012), viscous disc time scales are long enough to maintain Sgr A* feeding via an accretion disc for at least a million years. Furthermore, Nayakshin et al (2012, ApJ submitted) show that AGN feedback is unable to remove gas discs *within* the black hole's sphere of influence. Physically, this result is easily understood: escape velocities for gas in the sub-parsec scale disc are much larger than that for gas in the bulge of the host, so much more energy needs to be expended to eject gas from very near the black hole than from the bulge of the Galaxy. This is why a relatively low mass sub-resolution reservoir of gas (an accretion disc) could power Sgr A* for the duration of the quasar outburst envisioned here, while in the meantime Sgr A* drives much more massive outflows on scales of the Galaxy's bulge.

The outflow is believed to be self-regulating to have a scattering optical depth ~ 1 (King 2010a), so that the photons transfer their momentum to the outflowing wind which carries momentum

$$\dot{M}_{\text{out}} v \simeq \frac{L_{\text{Edd}}}{c}, \quad (1)$$

where $v \sim \eta c$, and $\eta \simeq 0.1$ is the accretion efficiency. We note that the mass outflow rate from Sgr A*, \dot{M}_{out} , is bound to be of the order of $\sim \dot{M}_{\text{Edd}}$, which is negligible on the Galactic scales, implying that we can neglect injection of the mass into the Galaxy (but not the outflow's momentum or the energy, as we discuss now).

2.2 The effects of the outflow on the diffuse gas in the Galaxy

Since the outflow velocity is very much larger than the escape velocity from the Galaxy, the outflow propagates with an approximately constant velocity until it shocks against the ambient gas. For a sufficiently powerful outflow, the shocked wind continues to drive an outflow outward, clearing the inner regions of the bulge of gas. The $M_{\text{BH}} - \sigma$ relation for elliptical galaxies and classical bulges may have been established by such outflows that terminated both host galaxy and SMBH growth (King 2005).

The point that we want to emphasize now is that even SMBHs lying well below this relation can drive the gas out of their host bulges, provided that the gas density is lower than that expected in the gas rich era when the bulge itself forms (King 2003, 2005). In our model, gas density in the bulge is parametrised through the gas fraction f_g :

$$\rho_g = \frac{f_g \sigma^2}{2\pi G R^2} = 2.5 \times 10^{-26} f_{-3} R_{\text{kpc}}^{-2} \text{ g cm}^{-3}, \quad (2)$$

where σ is the velocity dispersion in the bulge and R is the radial coordinate. The $\propto R^{-2}$ scaling of the density is natural as this is the same as that for the background stellar density that dominates the potential in the bulge. We further parametrize $f_g \equiv 10^{-3} f_{-3}$, $R = R_{\text{kpc}}$ kpc and we use the value $\sigma = 100$ km/s, appropriate for the Milky Way. For reference, the model of King (2003, 2005) assumes that $f_g = 0.16$, the cosmological value, during the bulge formation epoch.

The dynamics of the outflow depends crucially on whether the shocked wind cools efficiently or not. The shock temperature is of the order of 10^{11} K, so the only effective form of cooling is the inverse Compton effect of the shocked outflow's electrons on the Sgr A* radiation field (which would dominate over the whole Galaxy's light; Ciotti & Ostriker 1997). Outside a certain radius, R_{cool} , the radiation field is unable to cool the shock and the outflow transitions from momentum-driven to energy-driven (Zubovas & King 2012). This radius can be estimated by comparing the cooling and the flow timescales (King 2003). For the parameters of the Milky Way ($M_{\text{BH}} = 4 \times 10^6 M_{\odot}$), R_{cool} is

$$R_{\text{cool}} \simeq 12 f_{-3}^{1/2} \text{ pc}. \quad (3)$$

Even for the cosmological gas fraction ($f_{-3} = 160$), R_{cool} is very small compared with the size of the bulge. For the problem at hand, where the gas density in the bulge is likely to be much smaller than this, this implies that for all the relevant parameter space any outflow from Sgr A* quickly becomes energy-driven. In this type of outflow, almost all of the kinetic power of the outflow,

$$\dot{E}_{\text{out}} = \frac{1}{2} \dot{M}_{\text{out}} v^2 = \frac{\eta^2 c^2}{2} \dot{M}_{\text{out}} = \frac{\eta}{2} L_{\text{Edd}}, \quad (4)$$

is passed to the ambient gas, heating and pushing it outward. The shocked shell rapidly (in $t \lesssim 10^5$ yr) attains a constant velocity, which for a spherically symmetric outflow is given by

$$v_e = \left[\frac{2\eta\sigma^2 c}{3} \frac{0.16}{f_g} \frac{M_{\text{BH}}}{M_{\sigma}} l \right]^{1/3} \simeq 1920 \sigma_{100}^{2/3} f_{-3}^{-1/3} l^{1/3} \text{ km s}^{-1}, \quad (5)$$

where M_{σ} is the value of the SMBH mass expected from the $M - \sigma$ relation (King et al. 2011), $M_{\text{BH}} \simeq 0.2 M_{\sigma}$ and $l \sim 1$ is the Eddington ratio.

Once the quasar switches off, the shell continues to expand, but stalls and eventually stops (assuming that the isothermal potential of the bulge extends to infinity). The maximum radius which the shell reaches is

$$R_{\text{stall}} \simeq \frac{v_e}{\sigma} R_0 \simeq \frac{v_e^2}{\sigma} t_q, \quad (6)$$

where t_q is the duration of the quasar outburst.

Using the size of the observed *Fermi* bubbles ($R_{\text{stall}} \gtrsim 10$ kpc) we can constrain the free parameters of our model, f_{-3} and t_q . We estimate the gas fraction from equation (5), requiring that the bubbles must have reached the present radius in 6 Myr. This is equivalent to assuming that the shell's mean velocity is $\langle v \rangle \gtrsim 1600$ km/s (see Paper I for details), and yields

$$f_{-3} \lesssim \left(\frac{1920}{1600} \right)^3 l \simeq 2l. \quad (7)$$

We see that the gas fraction in the Milky Way halo must have been similar to 10^{-3} in order for the bubbles to be inflated within our model. Numerical simulations below confirm this.

Requiring that the bubble stalling radius should be greater than their current radius, equations (6) and (5) give

$$t_q > 2.5 \times 10^5 f_{-3}^{2/3} \text{ yr}. \quad (8)$$

As the bubbles are likely to be still expanding at the present time (see Paper I), this result is a lower limit. We note that the estimate given by equation 8 is a factor of 5 larger than the estimate obtained in Paper I. As both estimates are lower limits on the outburst duration, only the larger one of the two is relevant.

In 0.25 Myr, Sgr A* accreting at its Eddington limit consumes $\Delta M \simeq 2 \times 10^4 M_{\odot}$ of gas. Within our feedback model, $\sim 2 \times 10^{56}$ erg is ejected in the outflow's mechanical energy. This is more than an order of magnitude larger than the bubbles energy content estimated by Su et al. (2010). However, we find that a large fraction of the outflow's energy goes into mechanical work expended to drive the ambient cooler medium away from the Galaxy's centre. Zubovas & King (2012) show that even while the quasar driving is on, only 1/3 of the energy input is retained in the shocked wind while the quasar is active. When the quasar turns off, the bubble expands adiabatically, converting its thermal energy into kinetic energy of the bubble and the surrounding shell. Therefore it is likely that the actual amount of energy retained by the bubbles is much lower than the original energy input by Sgr A* into the outflow, bringing the value in line with the observations. Our simulations confirm this prediction; cf. §5.3.

2.3 The role of the Central Molecular Zone in focusing the outflow

The shell expansion velocity, v_e , depends on the gas density in the direction of expansion. Clearly, if the ambient gas distribution is not spherically symmetric then the outflow must lose its spherical symmetry too. As a minimum effect, the velocity of the contact discontinuity must be smaller in the directions of denser gas. The most salient feature in the distribution of gas in the inner Galaxy is that a good fraction of it – mainly the cold molecular gas – lies close to the plane of the Galaxy. For what follows it is the Central Molecular Zone (CMZ; Morris & Serabyn 1996), a massive disc-like molecular gas feature in the inner ~ 200 pc, that matters the most. As we argued in Paper I, the CMZ presents an almost impassable barrier to the Sgr A* outflow. This can be seen from the fact that the weight of the CMZ,

$$W_{\text{CMZ}} \sim \frac{GM_{\text{enc}}M_{\text{CMZ}}}{R_{\text{CMZ}}^2} = \frac{2M_{\text{CMZ}}\sigma^2}{R_{\text{CMZ}}} \sim 6.5 \times 10^{34} \text{ dyn}, \quad (9)$$

where R_{CMZ} is the mean radius of the CMZ and M_{enc} is the mass enclosed within this radius, is greater than the momentum flux impacting on the CMZ from Sgr A* outflow (which is the outward force on the CMZ):

$$F_{\text{CMZ}} \sim \frac{L_{\text{Edd}}}{c} \frac{H_{\text{CMZ}}}{R_{\text{CMZ}}} \sim 2 \times 10^{33} \text{ dyn}. \quad (10)$$

Therefore we expect the CMZ to be a very effective obstacle to the outflow (this estimate does not take into account energy deposition by the outflow into the CMZ, which makes the latter somewhat more prone to the feedback; see §5.6). Physically, we expect Sgr A* outflow impacting the CMZ to shock and thermalise. As the CMZ weight is so large, the outflow is either completely stopped or nearly stalled in the plane of the Galaxy. The shocked outflow gas cannot simply pile up there, however. Indeed, if that were the case then the pressure (thermal energy density) would increase in that location without limit. The thermal pressure of the shocked gas in the directions perpendicular to the Galactic plane is much lower because the outflow proceeds in those directions easily. Thus there is a strong pressure gradient in the shocked outflow gas pointing towards the Galactic plane. This pressure gradient clearly must launch a “secondary” thermally driven outflow away from the Galactic plane, efficiently collimating Sgr A* outflow into these directions.

3 SIMULATION SETUP

3.1 Numerical method

Our workhorse code for solving gas dynamics in the fixed potential of the bulge and the black hole is GADGET-3, an updated version of the code presented in Springel (2005). Feedback from the SMBH is implemented with the ‘virtual particle’ method explained in detail in Nayakshin et al. (2009). Rather than hydrodynamically modelling the low-density fast wind flowing from the SMBH, its effects on the gas distribution at large are simulated via a distinct population of particles, called ‘virtual particles’ since they exist only during their propagation from the source, Sgr A*, to the point of interaction with the ambient gas. These particles are ejected isotropically from the SMBH at each of

its timesteps and move radially with a set constant velocity ($v_w = 0.1c$). Each particle carries linear momentum

$$p_\gamma = \frac{L_{\text{Edd}}t_{\text{BH}}}{cN_\gamma} \quad (11)$$

and kinetic energy $E_\gamma = p_\gamma v_w/2$, where t_{BH} is the SMBH timestep, and divided equally among N_γ virtual particles ejected in that timestep. The scheme is designed to eject the correct momentum flux from the SMBH, L_{Edd}/c , and the number of particles ejected in a time step, N_γ , is selected so that the interactions with SPH particles are sufficiently frequent to reduce the (random-number-generated) noise to acceptable levels (see Nayakshin et al. 2009).

Each virtual particle has a search radius (a multiple of the smoothing length of an SPH particle), within which search for potential SPH neighbors is performed “on the fly”. Whenever an SPH particle kernel contains a virtual particle, the two are considered interacting, and a fraction of the virtual particle’s momentum and energy is transferred to the gas. When the virtual particle energy drops below 1% of its original energy, the particle is destroyed.

The kinetic energy of the virtual particles is passed to the SPH particles if the shocked wind does not cool, i.e. if $R > R_{\text{cool}}$ (eq. 3). We have implemented a step function transition between the pure momentum feedback regime and the energy feedback one for this. However, testing showed that since R_{cool} is very small in the case considered here, there is no significant difference in results between simulations utilising the switch and those employing the energy feedback scheme throughout the simulation, so we use the latter below.

While we do not model hydrodynamically the reverse wind shock, which thermalizes the wind and creates a pressurized bubble that can expand adiabatically, we find that this process is somewhat mimicked in the simulations by low density gas that is present in the otherwise evacuated bubble. These particles predominantly originate on the surfaces of the Central Molecular Zone (see Sections 3.2 and 4.1.3 below), where they are heated to very high temperatures and rise to fill the voids; subsequently quasar wind heats these particles even further. The bubbles are found to be significantly overpressurized with respect to the surrounding gas. This allows the bubble to expand thermally as expected if the reverse shock were modelled by SPH (see Section 4.1 below).

In all the simulations presented below, we use an ideal equation of state for the gas. The gas pressure is given by $P = \rho kT/\mu$, where mean molecular weight, $\mu = 0.63m_p$ (assuming ionised gas of Solar abundance), k is the Boltzmann’s constant, and ρ and T are the gas density and temperature, respectively. In all simulations except for one, we employ the standard GADGET optically thin cooling prescription based on the Sutherland & Dopita (1993) cooling curves, in addition to heating from the virtual particles on the contact discontinuity of the bubble. In the only exception to this, simulation ‘Cool’ (see Table 1), we check the sensitivity of our results to the assumed cooling function by utilising the optically thin radiative cooling rates for gas ionised (and also heated) by the quasar radiation field as calculated by Sazonov et al. (2005), who also provided an analytical fit to the respective rates that we use here.

Test	f_g	$N_{p,halo}$	t_q/Myr	$\left(\frac{H}{R}\right)_{\text{cmz}}$	M_{cmz}/M_\odot	$N_{p,\text{cmz}}$	R_b/kpc	d_b/kpc	h_b/kpc	$v_v/\text{km s}^{-1}$	$v_h/\text{km s}^{-1}$
Base	10^{-3}	7.5×10^5	1	0.25	10^8	10^6	11.5	9	~ 1	1090	670
HR-low	10^{-3}	7.5×10^5	1	0.125	10^8	10^6	11.5	9	~ 1	1110	680
Cool*	10^{-3}	7.5×10^5	1	0.25	10^8	10^6	9.5	10	~ 1	820	650
Fg-low	4×10^{-4}	3.0×10^5	1	0.25	10^8	10^6	~ 15	~ 10	2.5	2560	610
Fg-high	4×10^{-3}	3.0×10^6	1	0.25	10^8	10^6	6	6	~ 1	220	400
Tq-low	10^{-3}	7.5×10^5	0.3	0.25	10^8	10^6	7	4	2	300	360
Both-low	4×10^{-4}	3.0×10^5	0.3	0.25	10^8	10^6	~ 7	~ 4	4	960	270
Mc-low	10^{-3}	7.5×10^5	1	0.25	10^7	10^5	7	8	2	330	470

Table 1. Simulation parameters and main results. From left to right, the parameters are: Test ID, gas fraction, number of SPH particles in the halo, quasar outburst duration, CMZ mass, CMZ scale height, number of particles in the CMZ. The results are: bubble height, width and distance between its lower edge and the SMBH; velocity of the swept-up ISM in the z direction at $x = y = 0$ and velocity of the swept-up ISM in the xy plane at the mid-height of the bubble; all five at 6 Myr.

* - Simulation ‘Cool’ is identical to ‘Base’, but includes a Sazonov et al. (2005) heating-cooling prescription.

Simulation snapshots showing density and temperature are plotted using an angle slice projection method presented in Nayakshin & Power (2010). Specifically, the gas column density projected over the y coordinate is calculated by

$$\Sigma(x, z) = \int_{-y(x,z)}^{y(x,z)} \rho(x, y, z) dy, \quad (12)$$

where the limits of the integration are given by $y(x, z) = r \tan \zeta$ and $r = \sqrt{x^2 + z^2}$. The angle ζ is chosen so that $\tan \zeta = 1/4$ throughout this paper. This projection method conveniently allows us to get an unobscured look into the inner parts of the simulation and yet have enough particles at the outer edges for a statistically meaningful figure to be derived when plotting. In addition, since most of the results presented in this paper are symmetrical around the z axis, the snapshot plots, where applicable, are divided vertically and show the surface density in blue-white on the left and temperature in red-orange on the right.

3.2 Galaxy model and initial conditions

The initial setup for the Galaxy consists of three components, described below and summarized in Table 1. The ‘Base’ model is the model which best reproduces the *Fermi* bubble observations (Su et al. 2010). We analyze this simulation in detail below, and study the robustness of our results by varying the free parameters of the model.

The whole computational domain is embedded in a static isothermal background potential with $\sigma = 100$ km/s. In the centre of the coordinate system, fixed in space, is the SMBH. While we do not model accretion onto Sgr A* in detail (cf. §2.1), occasionally SPH particles may get very close to the SMBH, especially closer to the end of the simulations when feedback from Sgr A* is turned off. To avoid very small time steps, and thus very high numerical costs, associated with these “uninteresting” particles, we remove them using the sink particle formalism if the SPH particles are closer than $r_{\text{sink}} = 0.1$ pc to Sgr A*. As explained above, Sgr A* is “turned on” at the start of each simulation, radiating at its Eddington limit for a duration t_q , which is a free parameter of the model. Most of the models presented here use $t_q = 1$ Myr (since this was found to give the best results), although we explore shorter outbursts as well.

As mentioned above, we position a massive disc of gas – the Central Molecular Zone (CMZ; Morris & Serabyn 1996) – in the plane of the Galaxy at a distance between $R_{\text{in,cmz}} = 5$ pc and $R_{\text{out,cmz}} = 200$ pc from Sgr A*. The inner radius is chosen so that the whole CMZ would be comfortably outside the sphere of influence of Sgr A* ($R_{\text{infl}} \sim 2$ pc), but still account for the yet smaller circumnuclear disc of gas, which is observed to lie between ~ 2 and ~ 10 pc from the centre (Guesten et al. 1987; Morris & Serabyn 1996). Our model CMZ has uniform temperature throughout, chosen to give the appropriate constant scale height aspect ratio ($H/R = 0.25$ or 0.125 , with a corresponding difference in the adopted temperature floor for the simulations). It is rotationally supported in the radial direction, with $v_{\text{rot}} = \sqrt{2}\sigma$. The radial density distribution follows a $\rho \propto R^{-2}$ power law, and the mass of the disc is set to $M_{\text{cmz}} = 10^8 M_\odot$ (approximately the upper limit from observational constraints), although we ran one simulation with a much lower CMZ mass. Despite the high mass of the CMZ, it is marginally stable to self-gravity, since the Toomre (1964) parameter $Q \sim 3.4$ for $H/R = 0.25$, and 1.7 even for $H/R = 0.125$. We note that we do not fine-tune the CMZ to be only marginally stable in the simulations; it is a natural outcome of using the observationally constrained CMZ parameters. This result is probably not a coincidence: massive cold discs are widely believed to be self-regulating to have $Q \sim 1$ (Goodman 2003; Thompson et al. 2005; Nayakshin et al. 2012). In principle, such a low Q parameter might lead to fragmentation. However, since we set the temperature floor in the simulations to be equal to the initial CMZ temperature, we do not expect a significant fragmentation to occur (Gammie 2001; Rice et al. 2005). This assumption is consistent with simulation results (see Sections 4.1.3 and 5.6 below). The SPH particle mass of the simulations is $M_{\text{part}} = 100 M_\odot$, giving a minimum mass resolution of $\sim 4000 M_\odot$.

Finally, there is a diffuse spherically symmetric gaseous “halo” extending between $r_{\text{in}} = 1$ pc and $r_{\text{out}} = 15$ kpc with density following the isothermal profile given by equation 2. The gas fraction f_g is a free parameter of our model and is varied between 4×10^{-4} and 4×10^{-3} in different tests, with the fiducial value of 10^{-3} for the ‘Base’ model (this corresponds to a particle density $6 \times 10^{-4} \text{ cm}^{-3}$ at $R = 5$ kpc; see the Discussion section for the validity of this choice for gas

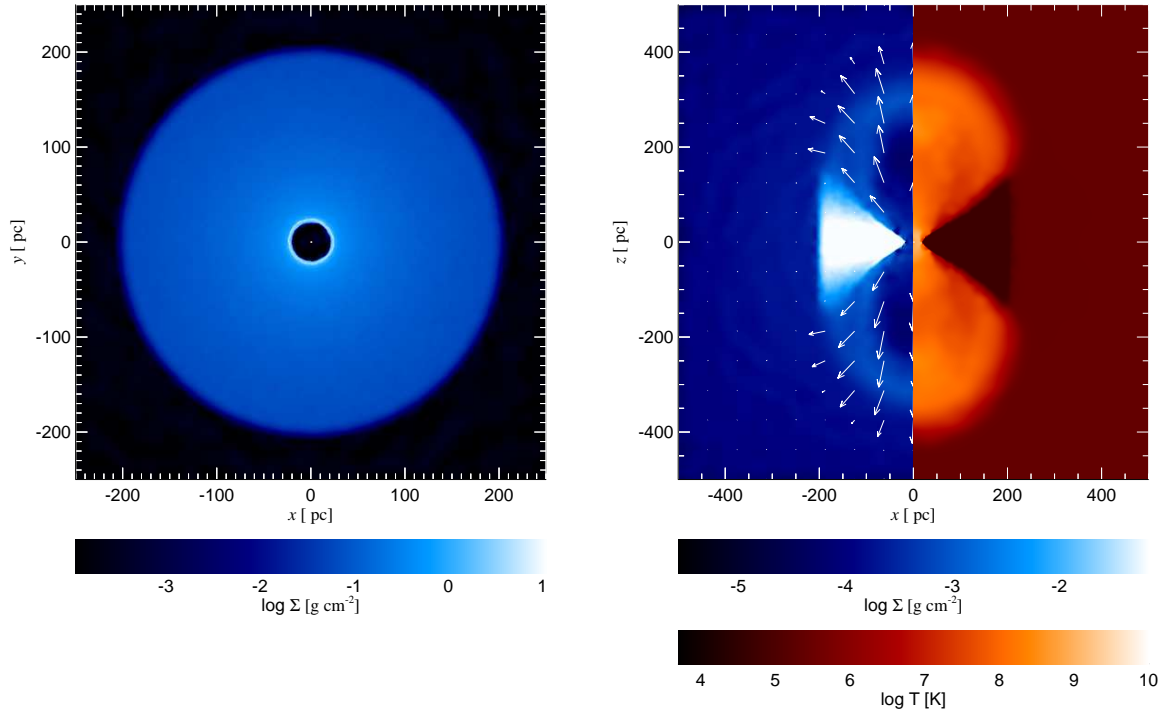


Figure 1. **Left:** The face-on column density of the CMZ disc at time $t = 0.1$ Myr for the ‘Base’ simulation. Note that the innermost region has been partially evacuated by Sgr A* feedback. **Right:** Cross-sectional plot of gas surface density (left half of the panel, blue-white) and temperature (right, red-orange) for the same snapshot. The CMZ (cold dense wedge in the Galactic plane) strongly collimates the outflow; even though its surfaces are ablated, teardrop-shaped cavities form readily.

density). The number of particles in the halo is set by their mass (we use same SPH particle masses for the CMZ disc and the halo). The gas temperature in the bulge halo is initially set to $T_{\text{halo}} = T_{\text{vir}} = 2.5 \times 10^5$ K, which corresponds to the virial temperature of the bulge. The initial gas velocity in the bulge is set to zero.

This halo setup we use is probably oversimplified. For example, we do not account for the likely anisotropy of the initial gas distribution of the “halo” due to overall rotation of the Galaxy. We address this point qualitatively in the Discussion section.

4 RESULTS

Table 1 shows the list, parameters and main results of all of the simulations that we present in this paper. Results of the three simulations in the top of the Table, separated from the rest by a horizontal line, appear to be a reasonable match to the *Fermi* Bubble observations by Su et al. (2010). The rest of the simulations produce bubbles that are unlike the observed ones.

We first describe the evolution and properties of the ‘Base’ model ($f_g = 10^{-3}$, $t_q = 1$ Myr).

4.1 Base simulation

4.1.1 Small and intermediate scales

Overall, the dynamics of gas in the simulation closely follows our analytical expectations. As soon as the quasar switches on, the spherically symmetric outflow hits both the CMZ and the halo gas. The left panel of Figure 1 shows the face-on view of the CMZ disc at time $t = 0.1$ Myr. Note that only the central ~ 25 pc of the disc were evacuated by outflow from Sgr A*. The right panel of the same figure shows the edge-on projections of both gas column density and temperature (which we present in a single panel because of the azimuthal symmetry of the gas flow). The arrows show gas velocity vectors projected on the plane of the figure.

As expected, the spherical “halo” (the diffuse gas component) is affected by the outflow much more than the CMZ, with the contact discontinuity between the wind and the shocked ambient medium at a distance of about 300 pc. We also note that the bubbles do contain some gas mainly closer to the interface with the upper layers of the CMZ. That gas is heated to temperatures above 10^8 K. There is a transition region between the almost-spherical outflow perpendicular to the Galactic plane and the stalled outflow against the CMZ, completing the figure-8 morphology of the whole flow.

As time proceeds the inner hole in the CMZ disc grows in size, engulfing most of the disc by the end of the simulation (see §4.1.3 for a fuller discussion of this). The cavities opened by the outflow in the directions perpendicular to the

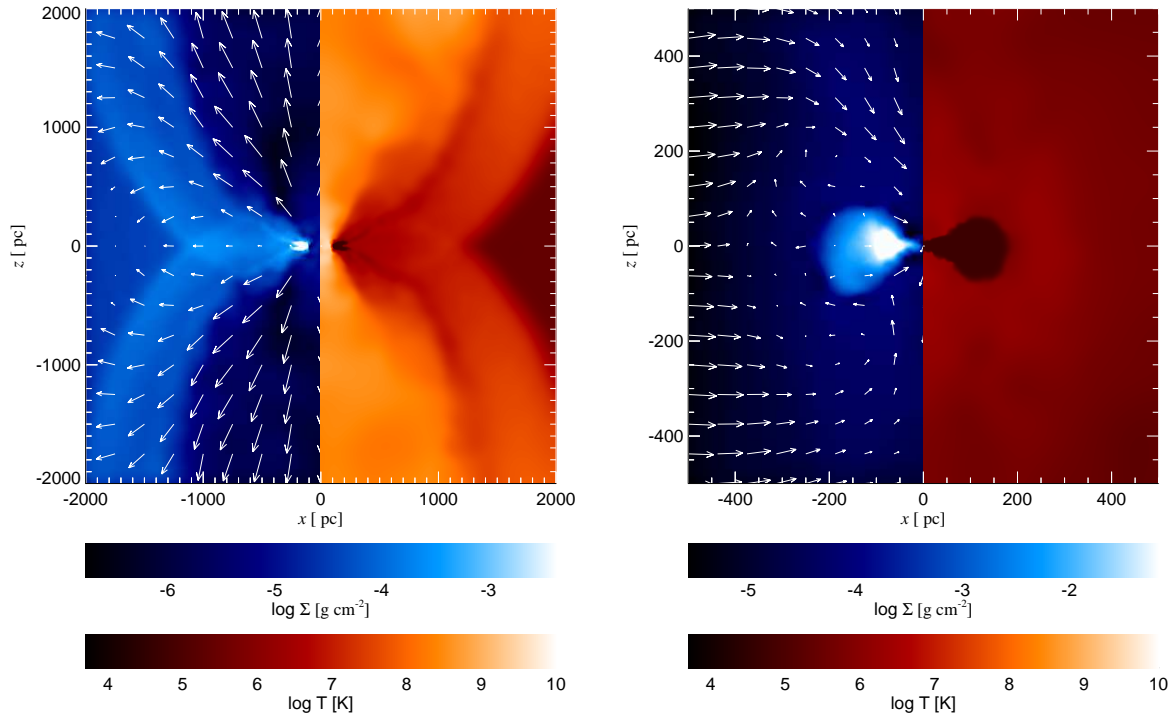


Figure 2. **Left:** Side view of gas surface density (left half of the panel, blue-white) and temperature (right, red-orange) in the central 2 kpc of the ‘Base’ simulation at $t = 1$ Myr. The CMZ has been enveloped by the external ISM shock fronts, but it still maintains the strong collimation of the diffuse cavities. The cavities are also filled with hot $10^8 - 10^9$ K gas, which allows them to expand in all directions once the feedback from Sgr A* has switched off. **Right:** Central 500 pc of the ‘Base’ simulation at $t = 6$ Myr. The CMZ remains, although its density structure is perturbed. There is also a “back flow” of warm ($T \simeq T_{\text{vir}}$) gas into the central regions, evacuated by the buoyant rise of the bubbles.

Galactic plane grow even more. The left panel of Figure 2 shows the edge-on view of the inner 2 kpc of the Galaxy at time $t = 1$ Myr. One notes the hour-glass shape of the cavities opened by the outflow, and a strong gradient in the outflow velocity with angle θ ($\tan \theta = |z/x|$) measured from the z -axis. In particular, the maximum velocity is reached at $\theta = 0$, such that velocity there is consistent with the analytical prediction of $v_e \sim 2000$ km/s, and the minimum is at $\theta = 90^\circ$. There is also a “failed” outflow around $\theta \approx 65^\circ$; gas flowing along these directions eventually falls on the Galactic plane, shadowed by the CMZ from further Sgr A* feedback. Some material is ablated from the surfaces of the CMZ. It expands and contributes to the tenuous gas filling the cavities.

The right panel of Figure 2 presents the edge-on view of the central 500 pc at the end of the simulation, at $t = 6$ Myr. Due to the relative buoyancy of the hot gas in the cavities with respect to the cooler “ambient” gas, the former leaves the region by that time, being replaced by the latter. This “back flow” of warm ($T \simeq T_{\text{vir}}$) gas returning to the central region after Sgr A* switched off is clearly seen in the pattern of velocity vectors on the left side of the right panel of Figure 2. We also point out that while the CMZ has been significantly affected by the outflow from Sgr A*, most of it remains in the region in the form of a ring discussed further in §4.1.3.

4.1.2 Large scales

We now discuss the larger scales of the “Base” simulation. Figure 3 shows the edge-on views of the simulation domain at times $t = 1, 3$ and 6 Myr (left, middle and right panels, respectively). The left panel in particular shows that by the time Sgr A* switches off the cavities are still rather small on Galactic scales: their height is $R \sim 3$ kpc and the maximum width is $d \sim 2.5$ kpc.

Further evolution of the hot bubbles is driven by the inertia of the outflow, the buoyancy of the bubbles and the fact that they are significantly over-pressurized with respect to the ambient medium (cf. the left panel of Figure 4). Bubble expansion proceeds in an almost self-similar fashion, except for a ripple at roughly the middle of the bubble height (see Fig. 3, middle panel). It is most likely a Kelvin-Helmholtz unstable mode which arises due to the material inside the bubble moving parallel to the surface of the contact discontinuity. The ripple rolls over and disappears by $t = 6$ Myr (Fig. 3, right).

By the end of the simulation, the cavities have expanded to reach a height of ~ 11.5 kpc (Fig. 3, right panel), consistent with the observed vertical extent of the *Fermi* bubbles (Su et al. 2010). The width, at ~ 9 kpc, is slightly larger than observed ($d_{\text{obs}} \sim 6$ kpc); we return to this point in the Discussion section. The cavities are filled with very hot ($T_{\text{bub}} \sim 2 \times 10^8$ K ~ 17 keV) and diffuse ($f_{\text{g,bub}} \sim 2 \times 10^{-5}$;

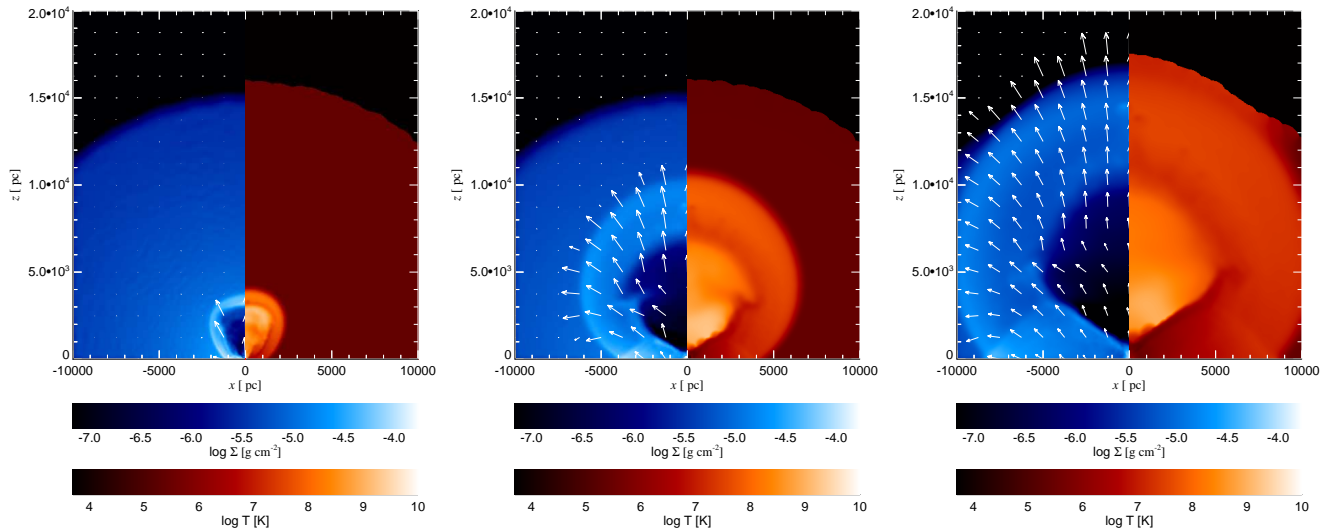


Figure 3. Gas evolution on large scales in the ‘Base’ simulation; the three panels correspond to $t = 1, 3$ and 6 Myr, from left to right. Only the positive- z side of the computational domain is shown, due to symmetry around the Galactic plane. The CMZ strongly collimates the outflow and allows the formation of a teardrop-shaped cavity with a morphology very similar to that of the observed *Fermi* bubbles. The bubbles continue to expand and rise due to high pressure and low density, even once the feedback has switched off.

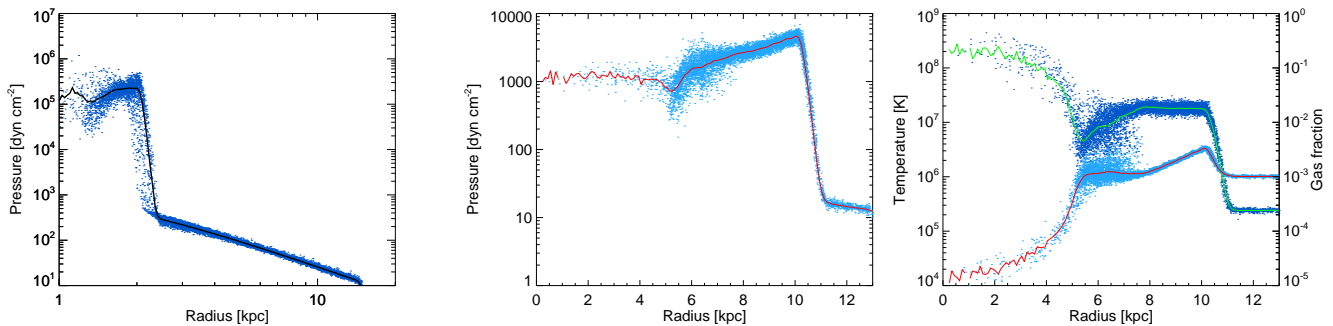


Figure 4. **Left:** Gas pressure as a function of cylindrical radius ($r_{\text{cyl}}^2 = x^2 + y^2$) for a selection of SPH particles at $1 < |z| < 2.5$ kpc (middle of the bubble) for the ‘Base’ simulation at $t = 1$ Myr; the solid line is the mean value at each radius. The central cavity is significantly overpressurised in comparison to the ambient medium, leading to lateral expansion of the bubbles. **Middle:** Same but at time $t = 6$ Myr when the bubble is much larger. The vertical cut chosen is now $4.5 < |z| < 6$ kpc. Note that the gas pressure has dropped significantly and is slowly varying across the bubble and the shocked region. **Right:** Temperature (green curve and dark blue points, left scale) and gas fraction (red curve and light blue points, right scale) against cylindrical radius for the same time and particle cut as the middle panel. The hot diffuse inner cavity and dense surrounding medium are obvious and have rather sharp edges (thickness ~ 1 kpc). Solid lines show mean values of gas fraction and temperature at each radius.

see Fig. 4, right) gas. For completeness, Figure 5 shows the time evolution of the bubble’s height, R , and width, d . The lateral expansion is initially somewhat faster than the vertical, possibly because some of the material expanding outward along the disc plane was blown off the top of the CMZ disc (rotating gas is easier to blow away due to centrifugal force). As is seen in the figure, in the next few Myr, the bubbles are as wide as they are tall at $t \sim 2$ Myr. Subsequently, vertical expansion becomes faster than lateral one. This may be driven by buoyancy: as the bubbles continue to rise up, their lower edges “lift off” from the plane, and the cooler gas can start flowing back along the plane.

The bubbles are slightly detached from the very centre of the Galaxy; the gradual increase in this detachment is

visible in Figure 3, and also in the right panel of figure 2. This detachment is caused by the bubbles rising buoyantly out of the Galaxy potential. By $t = 6$ Myr, the gap between the centre and the lower edges of the bubbles is $h \sim 1$ kpc, in agreement with observations that permit any value of the gap size below ~ 2 kpc (Su et al. 2010).

The left panel of Figure 4 shows the SPH particle pressure versus their cylindrical radius defined as $r_{\text{cyl}}^2 = x^2 + y^2$ selected at a slab of gas with $1 < |z| < 2.5$ kpc at $t = 1$ Myr, roughly corresponding to the midplane (i.e. half-height) of the bubbles at that age. We observe that the difference in pressure within the bubble and outside is greater than two orders of magnitude. This excess pressure continues to drive

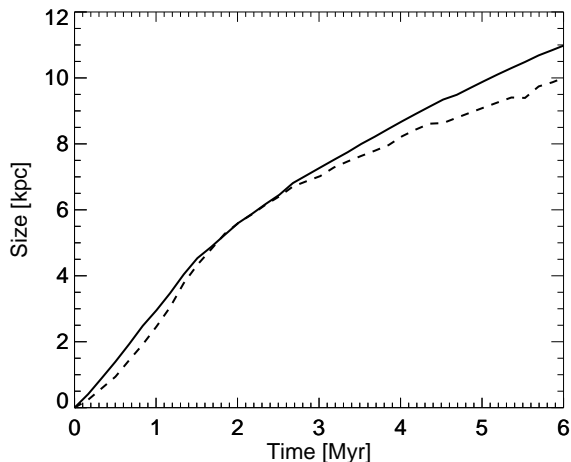


Figure 5. Height (solid line) and width (dashed line) of the bubbles as function of time in the ‘Base’ simulation.

the expansion in directions both parallel and perpendicular to the Galactic plane long after the quasar has switched off.

The middle panel of figure 4 presents the same as the left figure but at the end of the simulation and for a slab of material at a larger $|z|$ ($4.5 < |z| < 6$ kpc, corresponding roughly to the middle of the bubble that has now risen further from the Galactic plane at $t = 6$ Myr). Note that by $t = 6$ Myr, the gas pressure inside the bubble has dropped by two orders of magnitude; the pressure of the surrounding ISM is also lower, but only by about a factor 10, so the pressure difference between the bubble and its surroundings is much smaller. Consequently, the bubble expansion is much slower, as seen in Fig. 5 and the right panel of Fig. 3. The vertical expansion of the bubbles persists for longer due to residual momentum in the gas and buoyancy (see the last two columns in Table 1).

4.1.3 Feedback effects on the CMZ

In the simulation, we find that the CMZ is not dispersed by the outflow, a result consistent with the prediction of the analytical argument (cf. Section 2.3). However, the quasar wind is powerful enough to displace the inner ~ 120 pc of the CMZ to larger radii, resulting in formation of a dense thin ring (Figure 6, left).

The average radial expansion velocity of the inner parts of the CMZ, $v_{r, \text{cmz}} \sim 100$ km/s, is larger than the sound speed in its gas ($c_s \sim 20 - 40$ km/s, for $H/R = 0.125$ and 0.25 respectively) and comparable to its rotational velocity. Therefore some of the CMZ gas is shock-heated to $T \sim 10^6$ K and expands vertically. This allows the quasar wind to ablate the outer surfaces of the CMZ further. Gas from these regions fills the voids in the halo (cf. Sections 4.1.1 and 4.1.2, above). This process, however, removes only a small amount of mass: by the end of the simulation, the CMZ mass (defined as the gas mass within a radius 250 pc in the Galactic plane and within $z \pm 100$ pc) has decreased by less than 5%.

We would like to note another more significant dynamical effect of the Sgr A* outflow on the CMZ that re-shapes the initial disc configuration into a ring-like one. The out-

ward force and pressure of quasar wind cause a significant radial mixing in the CMZ. For example, some of the CMZ gas on the inner face of the disc is sent outward by the wind just above the surface of the outer regions of the disc, but stalls later on and falls back on the CMZ in the outer regions. This failed outflow has a small angular momentum in comparison to gas in the outer disc. The angular momentum of the CMZ gas is then well mixed up. This establishes a narrow distribution of specific angular momentum – a ring. We note that this mechanism of ring formation is similar in spirit to that found by Hobbs et al. (2011) in their simulation S30, although there shocks between material with different angular momentum were due to initial conditions in the collapsing gas shell rather than quasar feedback.

Subsequently, the ring slowly relaxes and spreads back somewhat into a disc configuration due to viscous stresses; however, the viscous timescale for this to happen at $R = 100$ pc is $t_{\text{visc}} \sim 10^8 (0.1/\alpha)$ yr for $H/R = 0.25$, where α is the standard Shakura & Sunyaev (1973) viscosity parameter. This is much longer than the timescales we are interested in, and thus unsurprisingly the ring persists to the end of the simulation (Figure 6, right).

Since the disc is only marginally gravitationally stable at the start of the simulation, it comes as no real surprise that the ring becomes more unstable than the original disc. As a result, some spiral density waves are visible in the middle panel of Fig. 6. Furthermore, a very massive dense clump forms at $t \sim 3.5$ Myr and there are hints of another forming by the end of the simulation at a position $\{x, y\} \sim \{80, -20\}$ pc. The radius of the clump is $r_{\text{cl}} \sim 5$ pc and its mass $m_{\text{cl}} \sim 10^7 M_{\odot}$. Its density is then $n_{\text{cl}} \sim 7 \times 10^5 \text{ cm}^{-3}$, ~ 500 times greater than the background potential density at the clump’s radial distance $R \simeq 100$ pc and similar to that of dense star forming molecular cloud cores. Due to the adopted temperature floor and lack of resolution in the simulations, the cloud cannot fragment into smaller globules, but we obviously expect such an object to be unstable to gravitational collapse. The result would presumably be a massive star cluster. The orbit of the clump around Sgr A* is mildly eccentric ($e \sim 0.2$). This may be interesting as a potential route to formation of the Arches cluster which has a rather non-circular orbit (Stolte et al. 2008) in particular, but it may be also relevant to the origin of other young Galactic Centre star clusters and GMCs (cf. further discussion in §5.6.3).

4.2 Dependence on the ambient gas density

The ambient gas density before Sgr A* quasar outburst is a free parameter of the model. Therefore, we varied f_g to see how our conclusions depend on this parameter. A fourfold increase in f_g (Simulation ‘Fg-high’, Fig. 7, left) results in a reduction of the bubble height by $\sim 40\%$ for the same t_q . This is consistent with the analytical prediction from equation (6) and can be understood in terms of the larger gas weight, which for an isothermal distribution is independent of radius and is

$$W_g = \frac{4f_g\sigma^4}{G} \quad (13)$$

(King 2003, 2010a). Denser gas weighs more, therefore requiring more energy to be lifted to the same height. Since

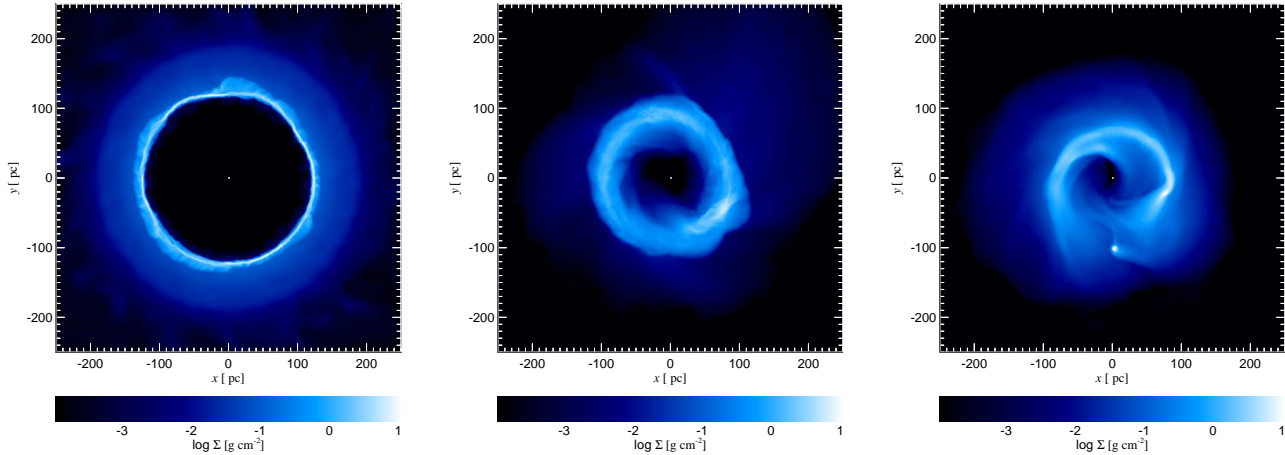


Figure 6. Density of gas in the central 250 pc of the ‘Base’ simulation at $t = 1, 3$ and 6 Myr (left, middle and right panels, respectively), as seen from above the Galactic plane. The inner regions of the CMZ are strongly affected by the quasar activity, forming a ring (left panel) which persists for several Myr (middle panel) while slowly spreading radially and developing unstable spiral filaments (right panel). A self-gravitating clump forms at $t = 3.5$ Myr, with another about to form by the end of the simulation. The total mass of the CMZ remains almost constant throughout the simulation.

the energy input is the same in both cases, higher values of f_g result in lower height reached by the bubbles. In fact, in simulation ‘Fg-high’, formally, the stalling radius of the bubble is $R_{\text{stall}} \sim 10$ kpc, similar to the size of the observed bubbles. However, the stalling time is $t_{\text{stall}} \sim 50$ Myr, which is much greater than the time since the hypothesized Sgr A* outburst. This shows that relatively high values of f_g are definitely disfavored within our model of a recent outburst origin for the *Fermi* bubbles (unless perhaps t_q is much longer than a 1 Myr; but see Section 4.3).

Conversely, a simulation with a lower gas density initial condition (‘Fg-low’, Fig. 7, middle) produces a bubble that is $\sim 40\%$ taller, but its interior temperature is rather low, blurring the distinction between the bubble and its surroundings. Furthermore, the lower density bubble rises further from the Galactic centre, producing a detachment $h_b > 2$ kpc, inconsistent with the data (Su et al. 2010). These disagreements allow us to exclude the possibility of a significantly lower gas fraction in the halo as well.

Our simulations show that the width of the bubbles, on the other hand, is almost independent of the ambient gas density. This is probably because the lateral expansion of the bubble is governed not only by the thrust from the outflow, but also by the pressure balance on both sides of the bubble (Fig. 4, left and middle panels). The ambient gas pressure increases with higher f_g , but so does the pressure inside the cavity due to lower bubble volume. The two changes compensate for each other, and the pressure inside the bubbles remains several orders of magnitude greater than in the external medium, leading to lateral expansion. Additionally, this expansion happens on an approximately dynamical timescale, which is given by the properties of the background potential and is also independent of f_g .

4.3 Dependence on the outburst duration

We now explore how simulation results depend on the outburst duration. Simulation ‘Tq-low’ (see Table 1) is identical to the ‘Base’ simulation except $t_q = 0.3$ Myr. As expected, lower t_q results in physically smaller bubbles (see Fig. 7, right panel). Due to a smaller amount of energy injected and a longer duration of adiabatic expansion phase after quasar switch off, the contrast between the temperature and density in the bubble interior and the surrounding shell is also smaller. The bubbles do have lower densities (effective $f_g \sim 4 \times 10^{-4}$, compared with the ambient $f_g \sim 10^{-3}$) and somewhat higher temperatures ($T_{\text{bub}} \sim 10^7$ K) than the surroundings, and thus do rise buoyantly away from the centre, resulting in large ($\gtrsim 3$ kpc by 6 Myr) separations of the bubbles from the centre. Vertical expansion of the bubble, however, is slower than in the ‘Base’ simulation; the outer edges of the bubbles reach only $\sim 5 - 6$ kpc by the end of the simulation. In addition, the bubble width is significantly smaller than in the ‘Base’ simulation, since a lower energy input results in a lower pressure inside the bubble, therefore lateral expansion is also slower.

This result provides a rough lower limit to the quasar outburst duration required to inflate the bubbles: $t_q > 0.3$ Myr, and quite likely $t_q \sim 1$ Myr. This is compatible with the analytical results, where we found $t_q > 2.5 \times 10^5$ yr from morphological arguments. We discuss this point further in the Discussion section.

Given that a lower value of t_q produces smaller bubbles, while a lower value of f_g increases their size (cf. Section 4.2), is it possible that reducing both t_q and f_g may yield as good or better morphological fit to the observed bubbles as the ‘Base’ simulation? We run a simulation to test this idea (see simulation ‘Both-low’ in Table 1), but find results incompatible with observations. Figure 9 shows the surface density

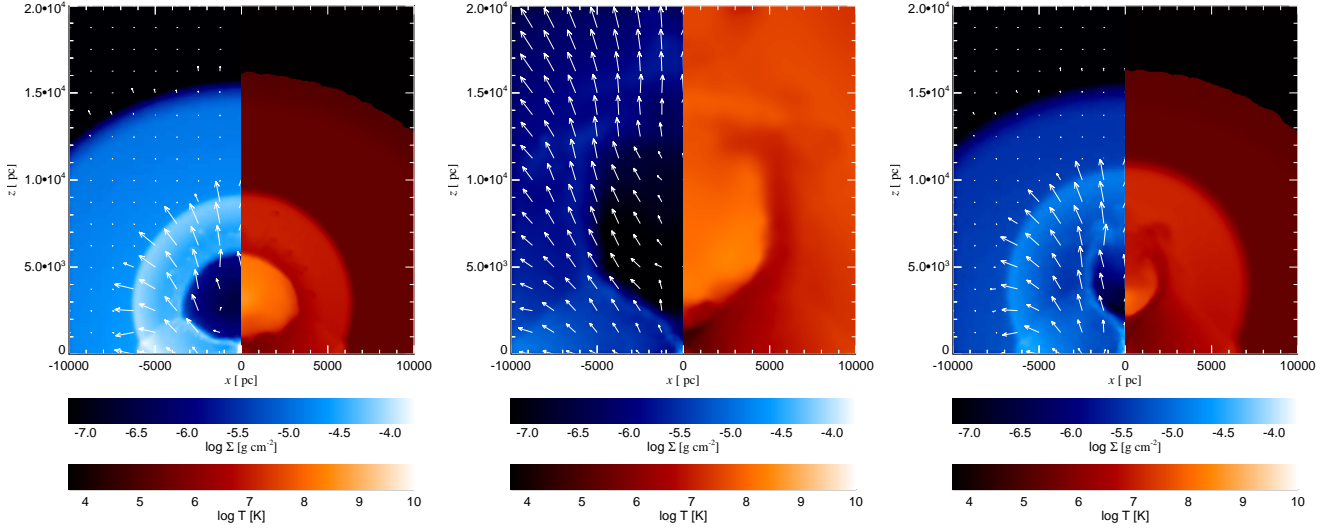


Figure 7. Density and temperature plots at $t = 6$ Myr of simulations with varying parameters. **Left:** higher gas fraction $f_g = 4 \times 10^{-3}$ (‘Fg-high’). **Middle:** lower gas fraction $f_g = 4 \times 10^{-4}$ (‘Fg-low’). **Right:** lower quasar outburst duration $t_q = 0.3$ Myr (‘Tq-low’).

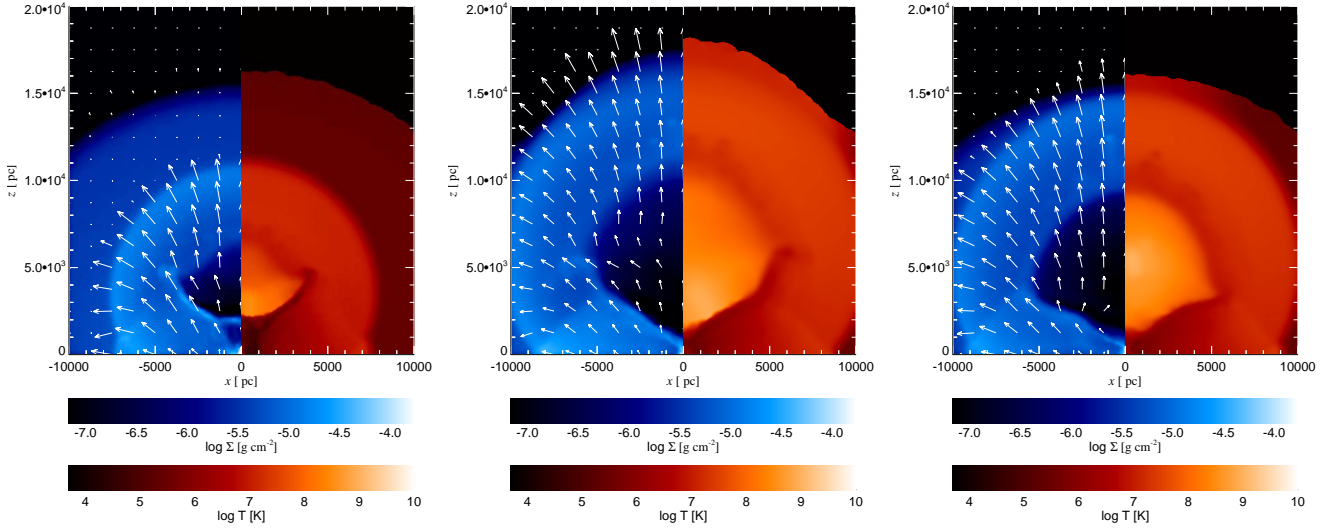


Figure 8. Density and temperature plots at $t = 6$ Myr of simulations with varying parameters. **Left:** CMZ mass decreased by a factor 10 (‘Mc-low’). **Middle:** CMZ aspect ratio decreased to $H/R = 1/8$ (‘Hr-low’). **Right:** a different heating-cooling prescription has been used (‘Cool’).

and temperature projections at the end of the simulation. While the height of the bubbles is comparable to that found in the ‘Base’ simulation, the width is too narrow. Also the gap between the Galactic centre and the lower edge of the bubbles is too large, and the morphology of the whole region appears too non-uniform compared with the observations by Su et al. (2010).

Increasing both t_q and f_g simultaneously by a factor larger than a few is also not a viable option. Morphologically, had the CMZ been able to withstand onslaught from Sgr A* feedback for longer, the dynamics of the gas may have produced reasonably shaped hot bubbles. But we are already using a CMZ mass that corresponds to the upper

limits derived from observations (Morris & Serabyn 1996), and even with $t_q = 1$ Myr the CMZ is significantly affected in the ‘Base’ simulation. It appears to us that increasing t_q further may do too large a damage to the CMZ, i.e., drive most of it to much larger distances from the Galactic Centre than it currently observed. Therefore we feel that t_q longer than ~ 1 Myr are not very likely, although there remains a possibility that the current CMZ is only a remnant of an even more massive gas disc that preceded the Sgr A* quasar outburst.

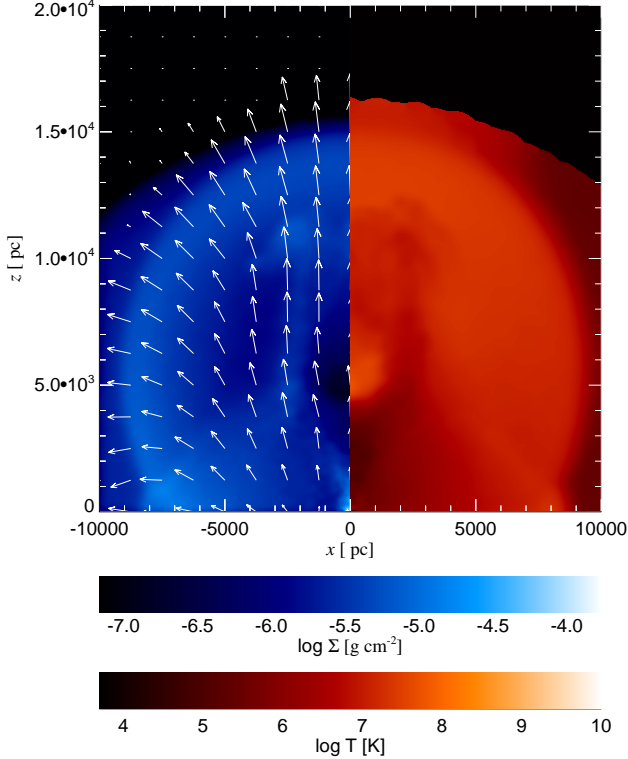


Figure 9. The structure of the bubbles at the end of the simulation ‘Both-low’ in which both the duration and background density of gas are reduced from that of the ‘Base’ simulation to $t_q = 0.3$ Myr and $f_g = 4 \times 10^{-4}$. The morphology of the bubble produced in this simulation is inconsistent with the observations.

4.4 Dependence on the CMZ properties

Having checked the effects of varying the halo and quasar parameters, we now vary the properties of the CMZ. In simulation ‘Mc-low’, we reduce the CMZ mass by a factor of 10, making it smaller than the current observational estimates ($M_{\text{cmz}} \sim 3 - 5 \times 10^7 M_\odot$; Dahmen et al. 1998; Pierce-Price et al. 2000).

The results are shown in Fig. 8, left. Comparing the figure with the right panel of Figure 3, we note that the shape of the bubbles and the shocked region is closer to spherical in the case of a less massive CMZ. Although the lower CMZ mass still yields a weight ~ 5 times larger than what the quasar outburst should be able to lift, the vertical density stratification in a homogeneous disc makes a large part of the CMZ diffuse enough to be blown away. The rest of the CMZ is shock-heated to higher temperatures than in the ‘Base’ simulation and begins to expand vertically, providing more material that can be removed by the wind. As a result, most of the CMZ is blown away by ~ 0.7 Myr in simulation ‘Mc-low’, and the outflow proceeds quasi-spherically for the last 0.3 Myr of the quasar activity. Although almost all of this material eventually accretes back onto the reforming CMZ disc after the quasar has switched off, the effects on the diffuse “halo” gas are profound. The bubble height is $\sim 40\%$ lower, their width is $\sim 20\%$ smaller and the bubbles are significantly detached from the Galactic centre. This

simulation does not appear to match the morphology of the *Fermi* bubbles as well as the “Base” simulation does.

We next check the influence of the CMZ geometry by reducing its scale height to yield the geometrical aspect ratio of $H/R = 0.125$, with a corresponding decrease in the temperature floor of the simulation (‘HR-low’, Fig. 8, middle). This value is smaller than the CMZ aspect ratio favored by the current observations ($H/R \sim 0.15$; Pierce-Price et al. 2000; Jones et al. 2011), so that we effectively cover all the reasonable parameter space in terms of H/R for the CMZ.

We find no qualitative difference between simulations ‘HR-low’ and ‘Base’. This suggests that even if the exact geometry of the CMZ plays a role in determining the bubble shape, the magnitude of this effect is quite limited. In all simulations, the bubbles are collimated much more strongly than pure shielding by the CMZ would suggest (the opening angle of the bubbles is $\Omega_b \sim 0.4 \times 4\pi$, while the solid angle not obscured by the CMZ in the ‘Base’ simulation is $\Omega_{\text{cmz}} \sim 0.8 \times 4\pi$), therefore this lack of difference is not particularly surprising.

4.5 Effect of the heating-cooling prescription

Simulation ‘Cool’ is identical to the ‘Base’ simulation, except that we use a physically motivated optically thin quasar heating-cooling prescription (Sazonov et al. 2005) instead of the standard Sutherland & Dopita (1993) one, as in the other simulations in this paper. The prescription is based on a fit to the radiative heating and cooling rates of the gas illuminated by a typical quasar radiation field. The radiative processes include photoionization heating, Compton and inverse-Compton processes, bremsstrahlung and line cooling, and assume an optically thin medium, which is well justified for the low column densities that we find in this paper, $\Sigma \lesssim 10^{-4} \text{ g cm}^{-2}$. The only region where gas may become optically thick to X-rays from Sgr A* is the mid-plane of the CMZ disc. However, we find that the higher density gas is able to cool efficiently anyway, thus staying close to the imposed temperature floor of $T = \text{a few times } 10^4 \text{ K}$ in any event.

The overall effect of changing the heating-cooling prescription on the large scale gas distribution is small (Fig. 8, right). The bubble interior is $\sim 50\%$ hotter ($T_{\text{bub}} \sim 3 \times 10^8 \text{ K}$ as opposed to $2 \times 10^8 \text{ K}$ in the ‘Base’ simulation), most likely due to less efficient cooling in the adopted prescription at $t > t_q$. The temperature of the outer shell is practically the same. Morphologically, this difference results in bubbles that have $\sim 10\%$ lower height and practically the same width, although the KH-unstable ripples are missing. The bubbles are also somewhat less collimated, as the material close to the Galactic plane is able to cool down more efficiently and collapse to higher densities. In general, however, the bubbles look rather similar. This shows that our results are somewhat insensitive to the details of gas heating and cooling. This finding is also consistent with the analytical predictions of King (2010a) and King et al. (2011), where by construction an energy-driven outflow occurs when cooling of the shocked wind and the shocked ISM becomes inefficient; we comment on this result further in Section 5.3. The effect of the X-ray heating from Sgr A* on the CMZ material is even smaller than that on the diffuse ambient gas, as explained above.

We point out that this insensitivity to quasar photoionisation heating and radiative cooling is to be expected due to the low density and a rather short duration of Sgr A* outburst compared with typical cosmological conditions (Sazonov et al. 2005). At higher densities we would expect the structure of the ambient gas to be significantly dependent on the details of the cooling function employed in the simulations.

5 DISCUSSION

5.1 Summary of simulation results

In general, our numerical simulations appear to confirm the suggestion of Zubovas et al. (2011) that an Eddington-limited outburst of Sgr A* outflow is a promising way of explaining the morphology of the observed *Fermi* bubbles. Starting with the model for AGN feedback developed to explain the $M_{\text{bh}} - \sigma$ relation for classical bulges and elliptical galaxies (King 2003, 2005), the “typical” initial conditions for numerical simulations of AGN feedback (Nayakshin & Power 2010) needed to be amended only to account for (a) the lower present day gas content of the Milky Way (i.e., smaller “gas fraction” f_g); (b) the presence of a massive gas disc, the CMZ, in the plane of the Galaxy in the central 200 pc; (c) a finite duration of Sgr A* outburst, which is a free parameter of our model, and is small compared with a dynamical time in a host galaxy bulge.

Given this setup, we confirm that a spherically symmetric outflow from Sgr A* is collimated by a geometrically thin CMZ disc in directions perpendicular to the Galactic plane. The outflow then produces two teardrop shaped cavities that have sizes similar to the observed γ -ray emission features. We varied the free parameters of our model - the quasar outburst duration t_q and the gas fraction f_g - to constrain their values to $t_q \approx 1$ Myr and $f_g \approx 10^{-3}$. The former is plausible and has interesting implications for Sgr A* feeding (cf. §5.7 below). The latter is poorly constrained observationally but consistent with estimates by McKee (1990) and Sofue (2011).

The opening angles of the bubbles as seen from Sgr A* are $\Omega_b \sim 0.4 \times 4\pi$. This is significantly smaller than the solid angle not obscured by the CMZ in the ‘Base’ simulation ($\Omega_{\text{cmz}} \sim 0.8 \times 4\pi$), showing that CMZ casts a larger “feedback shadow” than could be expected based on its geometrical aspect ratio alone. This is driven by the following two effects. First of all, the CMZ not only hinders the outflow propagation directly through it, but also “reflects” part of the outflow. The thermally driven outflow of hot gas ablated from the CMZ surfaces away from the Galactic plane redirects the gas flowlines towards vertical directions. Secondly, the bubbles rise due to buoyancy, and cooler material streams to fill the void along the Galactic plane, further reducing the opening angle of the bubbles.

In addition, although we were not originally interested in the evolution of the CMZ due to Sgr A* feedback – the role of the CMZ in our simulations was to stop and redirect the quasar wind only – we found several CMZ-related results interesting from an observational point of view: (a) re-shaping of the CMZ into a ring-like structure, perhaps explaining Herschel observations that CMZ is a dusty ring

rather than a disc; (b) an induced star formation mode in the CMZ which is triggered by Sgr A* feedback. These points are further discussed in §5.6.

We now make a detailed comparison of our results to observations.

5.2 Gas mass within the bubbles

In our simulations, two cavities corresponding to the observed *Fermi* bubbles are filled with hot and diffuse gas. The observationally estimated mass of gas within the bubbles ($M_{\text{bub}} \sim 10^8 M_\odot$; Su et al. 2010) is much greater than the mass of the shocked wind in our model. The latter, from analytical arguments in Section 2, is $M_w \simeq \dot{M}_{\text{Edd}} t_q \sim 8 \times 10^4 M_\odot$ for $t_q = 1$ Myr. The mass contained inside the cavities is $M_{\text{bub, sim}} \sim 6 \times 10^5 M_\odot$ for the ‘Base’ simulation. The density of gas within the bubbles ($n_{\text{bub}} \sim 3 \times 10^{-5} \text{ cm}^{-3}$) is also much lower than the one typically adopted in spectral modelling of the bubble emission ($n \sim 10^{-2}$, Su et al. 2010; Crocker & Aharonian 2011).

We believe that our simulations underpredict the gas density inside the bubbles which would otherwise be obtained in a more sophisticated simulation. We use a one-phase model for the ambient medium, whereas observations of gas in the Milky Way show that it is multi-phase (Dame et al. 2001). We would thus expect some cold and warm gas to be present even at large heights above the disc before Sgr A* “turns on”. Much like in supernova shocks expanding into the ambient medium, molecular clouds embedded in the ambient gas are expected to be overtaken by the quasar wind and later evaporate inside the bubbles, increasing the hot gas density there at late times (e.g. McKee & Cowie 1975). In addition to that, having strong density inhomogeneities in the ambient medium should provoke strong Rayleigh-Taylor instabilities (King 2010b) during the quasar outburst event, which we do not model here. These may allow formation of dense filaments resilient to Sgr A* feedback that are left behind the shock just like the molecular clouds discussed above. We hope to explore these ideas with improved simulations in the future.

5.3 Bubble energy content

The total energy input by the quasar into the system is

$$E_{\text{in}} \simeq \frac{\eta}{2} L_{\text{Edd}} t_q \simeq 8 \times 10^{56} t_6 \text{ erg}, \quad (14)$$

where t_6 is quasar activity time in Myr and $\eta/2 = 0.05$ is the coupling efficiency of the energy-driven wind (eq. 4). As mentioned in §2, E_{in} is significantly larger than the observational estimate of the total gas energy content of the bubble: $E_{\text{bub, obs}} \sim 10^{54-55} \text{ erg}$ (Su et al. 2010). However, in our simulations, the injected energy E_{in} is split between the bubble and the surrounding shell. Even when the quasar is active, analytical calculations show that only 1/3 of the input energy remains inside the bubble (Zubovas & King 2012), and this value should decrease after the quasar has switched off, as the bubble cools due to expansion.

To quantify this further, we computed the fraction of energy injected into the ambient gas by Sgr A* and retained by the bubble in the ‘Base’ simulation as a function of time (other simulations show similar results). To this end, we first

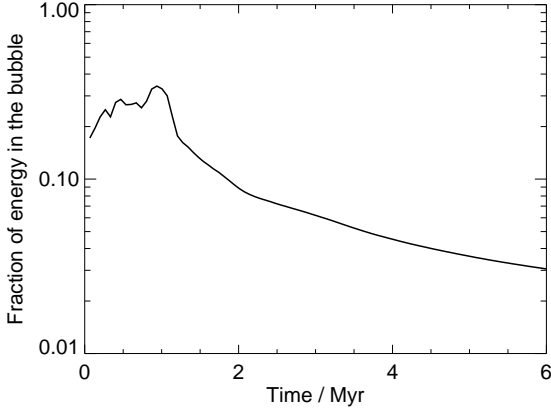


Figure 10. Time evolution of the fraction of energy input into the system by the quasar wind that is retained inside the bubbles. The rest of the energy is contained in the shell of shocked expanding ambient gas.

compute the sum of kinetic and thermal energy for all the gas particles in the simulation, $E_{\text{tot}}(t)$. We exclude in this calculation the gravitational potential energy of gas because for most SPH particles in the calculation changes in the latter are small compared with the changes in the kinetic and thermal energy. We then define the energy content of the gas within the bubble, $E_{\text{bub}}(t)$, as the sum of kinetic and thermal energy of the gas inside the bubble. The fraction of energy retained in the bubble is thus defined as

$$\epsilon_{\text{E,in}}(t) \equiv \frac{\Delta E_{\text{bub}}}{\Delta E_{\text{tot}}} = \frac{E_{\text{bub}}(t) - E_{\text{bub}}(0)}{E_{\text{tot}}(t) - E_{\text{tot}}(0)}. \quad (15)$$

Figure 10 presents the evolution of $\epsilon_{\text{E,in}}$ with time. While the quasar is active, the fraction of energy retained inside the bubble grows slightly and fluctuates around the analytically derived value of $1/3$. Once the quasar switches off, the expanding bubble cools and transfers most of its energy to the surrounding shell, so that by $t = 6$ Myr, only $\sim 3\%$ of the total energy input is retained inside the bubble. Hence the total energy content of the bubbles by the end of the simulation is

$$E_{\text{bub}} \sim 0.03E_{\text{in}} \simeq 2.5 \times 10^{55} t_6 \text{ erg}, \quad (16)$$

a value similar to but still a little larger than the observed one.

A further decrease in the bubble energy content may be caused by radiative cooling. To check this, we consider the evolution of $E_{\text{tot}}(t)$ and find that after $t = t_q$ it is conserved to within a few %. Adding a reasonably parametrized (using $r_s = 1$ kpc as a scale radius) value for the gas potential energy does not change the result either. Therefore the importance of cooling on the total energy content is minimal and does not affect our previous considerations.

5.4 Expected radiation from the bubble

The main emission components of interest are the γ -ray emission from the lobes (Su et al. 2010), a tentative microwave feature coincident with the bubbles identified in the WMAP all-sky maps (Finkbeiner 2004; Su et al. 2010) and

an X-shaped feature visible in the X-rays closer to the Galactic plane, coinciding with the edges of the bubbles, known as the “ROSAT limbs” (Snowden et al. 1997). We discuss each of the three components in turn.

While we do not model cosmic ray (CR) particles in our paper, we note that astrophysical shocks are known to accelerate electrons, protons and other particles to CR energies (Blandford & Eichler 1987) in a variety of environments and put as much as $\sim 10\%$ of the blast wave energy into the high energy particle component in the case of supernova shocks. We certainly do not see an obvious reason why shocks driven by an even faster outflow from a quasar would be less efficient in producing CRs than supernovae.

Two competing explanations for the origin of the γ -ray emission from the *Fermi* bubbles were suggested in the literature to date. Crocker & Aharonian (2011) suggested that the emission is powered by CR protons through pp collisions with the plasma in the bubbles. In this scenario, $\sim 10^{39} \text{ erg s}^{-1}$ of energy is injected into the bubbles in the form of CRs for $\sim 10^{10}$ yrs to achieve saturation in the system (cf. also Crocker 2011). This yields $\sim 3 \times 10^{58}$ erg in CR energy alone. This is some 3 orders of magnitude larger than the thermal energy retained within the bubbles in our “Base” simulation (equation 16). Therefore we conclude that our model is very unlikely to produce a bright enough γ -ray emission if emitting particles are hadrons.

On the other hand, Mertsch & Sarkar (2011) explore the possibility that electrons accelerated by shocks in turbulent plasma inside the bubbles can reproduce the spectral features, as well as the constant surface brightness profile. They find that this acceleration process can continuously replenish the energetic electron population, overcoming the problem of rapid electron cooling via the inverse-Compton process. The cooling time due to both IC and synchrotron losses is less than 5 Myr for 100 GeV electrons at $z = 5$ kpc above the Galactic plane (Fig. 28 and Section 7.1 in Su et al. 2010). Since the current γ -ray luminosity of the bubbles is $\sim 4 \times 10^{37} \text{ erg s}^{-1}$, and the age of the bubbles is 6 Myrs in our model, we conclude that at least $\sim 10^{52}$ erg of CR electrons is required to explain the *Fermi* Bubbles, and somewhat more if we account for continuous replenishment from plasma turbulence. This would be a very small fraction of the bubble energy content in our model, and on that basis at least is possible.

The origin of “continuous” shock driving inside the bubbles can be naturally explained by our model. Since the *Fermi* bubbles are still expanding at the end of the simulations, we expect that the whole volume of the cavities inflated by the quasar outburst is still filled with shocks. As noted in §5.2, a higher resolution modelling that includes a multi-phase description for the ambient pre-shock gas is likely to result in strong Rayleigh-Taylor instabilities of the wind shock front during the quasar outburst event (King 2010b). This should let cold gas filaments fall into the bubble’s interior due to gravity, leading to high Mach number shocks. Protons and electrons could thus be continuously accelerated on these shocks now, as suggested by Mertsch & Sarkar (2011).

The observed microwave haze spatially coincides with the *Fermi* bubbles, although its intensity decreases with height above the Galactic plane, especially in the southern bubble (see the bottom right panel of Figure 18 in Su et al.

2010). The luminosity of synchrotron emission from cooling electrons decreases with height above the plane possibly due to an expected decrease in the magnetic field strength. We believe that same electrons responsible for the γ -ray emission may be responsible for the WMAP haze.

The ROSAT-observed X-ray background in the region of the *Fermi* bubbles is composed of X-shaped ridges coincident with the lower limbs of the bubbles, most clearly visible in the hard (1.5 keV) band of the instrument, and a cavity in soft-band X-ray emission coincident with the bulk of the bubble area (Snowden et al. 1997; Su et al. 2010). The spatial coincidence of the features suggests a common origin.

In our simulations, gas inside the bubbles has temperatures as high as $\sim 10 - 20$ keV (see Figure 4, right) and so most of its thermal emission is harder than what ROSAT would detect. This could then explain the deficit of soft X-ray emission from within the bubbles. The shocked ISM (see Section 5.5 below) is heated to temperatures of a few times 10^7 K, (although that is expected to scale as $\propto \sigma^2$, so may vary somewhat if the model for the potential in the inner 10 kpc of the Galaxy is varied). The shocked shells around *Fermi* bubbles should then be most visible in the harder ROSAT bands. X-ray emissivity scales as $\propto n^2$, where n is gas particle density. The latter tends to be larger close to the Galactic plane due to superposition of the shells around the two bubbles (Figure 3, right) and vertical stratification. Therefore we may expect the lower limbs of the shells to be brighter in X-rays, as observed.

5.5 Bubble edges and the outer ISM shock

The expanding SMBH wind drives a strong forward shock into the ISM, which is expected to be adiabatic and move with $v_{\text{ISM}} \sim 4/3v_e$ (Zubovas & King 2012). Since the shell thickness is initially zero, its vertical extent should also be $r_{\text{ISM}} \sim 4/3r_b$, i.e. the thickness of the snowplough shell should be 1/3rd of the bubble height (Zubovas & King 2012). We note that in the simulations, it is somewhat greater: $d_{\text{sh}}/r_b \sim 0.4$. This result is not due to poor resolution. At late times, the thickness of the shell is ~ 10 times greater than the typical SPH particle smoothing length inside it ($h_{\text{SPH,sh}} \sim 500$ pc), therefore we believe the large-scale morphology of the region is well resolved.

The most likely reason for the discrepancy is the fact that the analytical model assumes a continuous quasar outflow driving the shell, whereas in our simulations the quasar turns off at $t = 1$ Myr. As a result the shell is less compressed in the radial direction.

In addition, our one-phase treatment of the ambient diffuse medium (cf. §5.2) can under-estimate the radiative cooling in the shell. Therefore, a more realistic multi-phase simulation could be expected to have thinner shell enveloping the *Fermi* bubbles.

Simulations also show transition regions at the edges of the bubbles (e.g. at $r_{\text{cyl}} = 4-5$ kpc in Figure 4, right). These are $\lesssim 1$ kpc thick zones where both temperature and density change from the values appropriate for bubble interior to those of the swept-up ISM. The observed bubble edges are $5 - 10^\circ$ wide, corresponding to a few hundred parsecs, in good agreement with simulation results. However, we must note that the SPH particle smoothing length in these regions

is comparable to the region thickness, therefore numerical effects probably dominate the result.

5.6 Has Sgr A* feedback affected the CMZ?

The primary goal of our paper is investigating whether Sgr A* feedback is a reasonable model for the morphology of the *Fermi* bubbles. In doing so we purposely introduced a very simple model for the CMZ – a $\Sigma(R) \propto R^{-1}$ circular disc in the plane of the Galaxy with mass and size consistent with observations (Morris & Serabyn 1996). This simple model nevertheless resulted in an interesting transformation and excitation of the CMZ that is worthy of further discussion.

5.6.1 The Herschel ring: a feedback-compressed disc?

In particular, we find that, under the strong coercion from Sgr A* feedback, the initial disk configuration of the CMZ attains a morphology more reminiscent of a dense ring (see Section 4.1.3 and Figure 6). We believe this is a general result of an AGN feedback acting on a disk since the physics behind this “anti-diffusion” evolution of the disk is simple and thus robust.

When the inner regions of the disc are blasted with an outward-directed feedback from the centre, little of the material outflows to infinity; most actually falls back onto the disc at large radii, mixes with gas there and thus induces an inward-directed radial flow at those radii. AGN feedback thus serves as an external agent that forces shock mixing of gas initially located at different radii and carrying different specific angular momenta. An initially broad distribution of angular momentum (a disc) becomes more narrow (a ring).

The slow viscous evolution of the dense ring that is formed by feedback suggests that such a ring should be still present in the GC today. In fact, recent *Herschel* observations of the GC region have revealed a ring-like structure on the scale of ~ 100 pc (Molinari et al. 2011), qualitatively similar to what we see in the simulations. The observed feature is elliptical and offset from Sgr A*. In Section 5.6.2 below we discuss how this strongly non-circular and offset structure could be formed in our model.

The fact that the CMZ is only perturbed but not dispersed to infinity is consistent with analytical predictions in §2.3. We note also that it may seem paradoxical how this very massive gas disc gets evacuated in the inner region and yet Sgr A* continues to accrete from presumably a much smaller disc at the assumed Eddington rate for ~ 1 Myr as in our “Base” simulation. However, the paradox is easily solved by realising that weight per unit mass of the gas – i.e., acceleration due to gravity – scales as $\propto M(R)/R^2$, where $M(R)$ is the total mass enclosed within radius R . The disc that fed Sgr A* may have had a radius of order $R \sim 0.1$ pc or even less (Nayakshin & Cuadra 2005; Alexander et al. 2012). The weight of the *accretion disc* of mass $M_d = 10^5 M_\odot$ is then

$$W_{\text{ac}} = \frac{GM_{\text{bh}}M_d}{R} = 1.2 \times 10^{36} M_\odot \text{ dyn}, \quad (17)$$

which is some ~ 20 times larger than that estimated for the CMZ (equation 9). It is thus perfectly reasonable that a smaller-scale disk would be too tightly bound to the SMBH to be expelled or even significantly perturbed by feedback,

unlike gas at larger radii. Nayakshin, Power & King (2012, ApJ submitted) show in their Appendix that this is a general point.

5.6.2 Non-circular orbit of the Herschel ring

Molinari et al. (2011) find that the Herschel ring is offset from Sgr A* and thus the centre of the Milky Way by about 50 pc, which is comparable with the size of the ring itself (see their figure 5). Any offset, and especially such a large one, is not naturally expected if the ring is a long-lived structure. While our model shows no offset, we note that there may be a natural way to produce that, although further numerical simulations are needed to confirm these ideas.

In particular, we have assumed here that the feedback from Sgr A* is exactly spherically symmetric. This is likely to be an over-simplification. Even if wind outflow is quasi-spherical on small scales (e.g., hundreds of Schwarzschild radii), on the somewhat larger scales of stellar discs we know that there must be an accretion disc which cannot be readily expelled by Sgr A* feedback as discussed above. We also know that the young stellar discs orbiting Sgr A* are not simple planar structures, with significant warps needed to explain the observed stellar kinematics (Bartko et al. 2009). Large warps also naturally occur in numerical simulations of star forming gas flows (Hobbs & Nayakshin 2009). Therefore, due to shadowing of Sgr A* feedback by the ~ 0.1 pc gas flow (which may be strongly non-circular), one side of the CMZ may have experienced a different amount of feedback compared with the other side, causing a strong non-axisymmetric perturbation to the CMZ disc and perhaps leading to an offset ring reminiscent of the observed Herschel ring. We note that the asymmetry in the feedback should not be too large over the whole 4π solid angle, however, so as to not result in too asymmetric *Fermi* Bubbles.

Additionally, natural non-axisymmetric density variations in the pre-feedback CMZ may result in outflow within the CMZ proceeding at different velocities in different directions, producing the offset.

5.6.3 Induced star formation in the CMZ?

A particularly interesting outcome of the CMZ compression by the outflow is the formation of a dense clump of gas at $t \sim 3.5$ Myr (see Section 4.1.3). The large mass, $\sim 10^7 M_\odot$, of the clump and its position at $R \sim 100$ pc from the Galactic centre suggest that the observed young Galactic centre stellar clusters (Serabyn et al. 1998; Figer et al. 1999a,b) or some of the largest molecular clouds (e.g. Sgr B2, Scoville et al. 1975; Reid et al. 2009) may have formed this way. Many smaller clumps in the dense ring may be susceptible to star formation; recent IR observations (Yusef-Zadeh et al. 2009; Immer et al. 2012) reveal that the star formation rate in the CMZ during the past ~ 1 Myr was $\sim 0.08 M_\odot \text{ yr}^{-1}$. At this rate, all of the CMZ gas would be turned into stars in $\sim 6 \times 10^8$ yr; even if the CMZ was supplied by molecular gas from further out, the whole molecular gas content of the Milky Way would have been turned into stars in ~ 6 Gyr. This suggests that the current star formation rate in the CMZ is higher than the long-term average, further implying a rather recent perturbation, consistent with the

results of our simulations. Furthermore, combined *Chandra* and *HST* observations have revealed a population of isolated massive (O and B giant, but also WR) stars in the CMZ (e.g. Mauerhan et al. 2010). These stars are not associated with any of the known clusters and may have formed in small associations. Our simulations suggest that while these stars are isolated now, they may have formed coherently in time if not in space due to a single very powerful perturbation produced by Sgr A* quasar outburst that turned the disc into a star-forming ring.

Finally, we note that the strong perturbations to the initially circular orbits of gas in the CMZ by Sgr A* feedback could form gas clumps on eccentric orbit. Indeed, the orbit of the clump found in the “Base” simulations is mildly eccentric, $e \sim 0.2$. That was obtained in a perfectly azimuthally symmetric simulation; any deviation from this assumption would have likely resulted in an even more eccentric clump. Such eccentric clump formation mechanism may be relevant to the origin of the Arches cluster which has a rather non-circular orbit (Stolte et al. 2008).

5.7 Implications for AGN feeding models

Sgr A* is the closest SMBH, and while its dimness is a familiar (and important) tale that stimulated development of non-radiative models of accretion for low density gas flows near SMBHs (e.g., Narayan et al. 1995; Blandford & Begelman 1999), little has been known about the past of Sgr A* as an accretion-powered SMBH. This is mainly due to potential difficulties of discovering signs of past Sgr A* activity. Light-echos due to X-ray fluorescence of Sgr A* radiation on molecular clouds is a powerful technique (Sunyaev & Churazov 1998; Revnivtsev et al. 2004; Terrier et al. 2010) but can only be used to constrain Sgr A* activity up to $\sim 10^4$ yrs at best due to the finite size of the Galaxy and the $\sim 1/R^2$ fading of signals from clouds at large distance R from the Galactic Centre.

However, shocks induced by an outflow from Sgr A* may continue to be visible for about a dynamical time of the Galaxy, i.e., $R_G/\sigma \sim 50$ Myrs, where we set Galaxy “radius” to be ~ 5 kpc and velocity dispersion $\sigma = 100 \text{ km s}^{-1}$ for illustrative purposes. Therefore, the *Fermi* lobes detected by Su et al. (2010) may be such a “shock-echo” of the past Sgr A* activity. Following Zubovas et al. (2011) we required the activity episode of Sgr A* to coincide with the well known star formation event in the Galactic Centre ~ 6 million years ago (Paumard et al. 2006), and found that the model has a number of attractive observational consequences which lend some support to this picture.

If Sgr A* indeed did have an Eddington-limited outburst for as long as ~ 1 Myr, it must have accreted $\sim 10^5 M_\odot$ of gas. This is an order of magnitude more than the mass in the stellar discs (Paumard et al. 2006; Nayakshin et al. 2006). The fact that Sgr A* managed to accrete $\sim 90\%$ of the gas from the star-forming accretion disc is highly significant for the general question of how SMBH are fed, and should be explored further as a potential example of an AGN disc that avoided “star formation catastrophe” in which gas is believed to be turned into stars too rapidly to feed AGN (Goodman 2003; Nayakshin et al. 2007).

5.8 Uncertainties and deficiencies of our work

As discussed in §5.4, we model the ambient gas “halo” with a single phase medium, whereas the ISM is expected to be multi-phase (McKee 1990). The lower density medium, essentially unresolved in our simulations, is probably quite important for the dynamics of the fast outflow from Sgr A* interacting with the gas in the bulge of the Galaxy (see also §5.2). Therefore some of our conclusions (e.g., the likely quasar phase duration t_q , the geometrical thickness of the shocked shell, etc.) may somewhat depend on the treatment of the ambient medium, and future work is needed to quantify this issue.

Also, a more realistic model for the geometrical arrangement of the diffuse “halo” gas that the outflow interacts with is desirable as this probably affects the eventual shape of the bubbles. In our simulations, we consider a spherical halo mass distribution, whereas in reality, we expect stratification on a large scale, with higher gas density in the Galactic plane than perpendicular to it, and higher density in the bulge than outside. We can make a very simple estimate of the magnitude of this effect by considering the dependence of outflow stalling radius on the gas fraction, which we take here to be the mean gas fraction along a direction of expansion. The analysis in Paper I and Section 2 shows that $R_{\text{stall}} \propto v_e^2 \propto f_g^{2/3}$. As the bubble expands in an approximately self-similar fashion (see Section 4.1) after the quasar switches off, we can estimate that in any given direction $R_{\text{bub}} \propto f_{g,\text{eff}}^{2/3}$. Therefore a factor of three difference in gas fraction results in approximately a factor of two difference in bubble radius. We hope that future observations of diffuse gas in the bulge of the Milky Way will help to constrain this part of our model.

Our results are, as expected, sensitive to the total mass of the CMZ, producing bubble morphology inconsistent with observations if it is reduced to $10^7 M_\odot$ or less. This low value of the CMZ mass is however unrealistically small, smaller than the current observational constraints of $3\text{--}5 \times 10^7 M_\odot$ (Dahmen et al. 1998; Pierce-Price et al. 2000). A potentially important caveat is that we model the CMZ as a smooth disc, rather than as a clumpy distribution of gas (Molinari et al. 2011; Morris & Serabyn 1996). In principle, a real outflow may stream past the clumps and so the collimation effect of the CMZ would be smaller than what we find. However, observations also show that the column density of gas toward the Galactic centre does not vary strongly with viewing direction (Goto et al. 2008), so the CMZ should provide a strong covering effect to any outflow coming from Sgr A*. In addition, we find that the CMZ aspect ratio has a negligible effect on the bubble properties, i.e. there is a range of CMZ column densities for which the outflow is collimated efficiently. Therefore, we believe that the uncertainty in our results due to the shape of the CMZ is relatively small.

6 CONCLUSIONS

We have presented numerical simulations of a wide angle outflow from Sgr A*, temporally coincident with the star formation event ~ 6 Myr ago, and collimated into directions perpendicular to the plane of the Galaxy by the presence of

a massive disc of gas, the Central Molecular Zone. Our main results are:

- This model is a plausible way to inflate the γ -ray emitting lobes recently observed by the *Fermi*-LAT, provided that Sgr A*'s outburst duration is $\lesssim 1$ Myr.
- The energetics of the model is consistent with the observed γ -ray emission if radiating particles are electrons rather than hadrons.
- Sgr A* feedback could have reshaped the CMZ from a disc-like configuration into a ring-like one reminiscent of the observed structure (Molinari et al. 2011). We speculate that somewhat asymmetric feedback could produce an observed offset of the ring and eccentric orbits for young star clusters such as the Arches star cluster.
- Furthermore, CMZ compression by the feedback outflow may explain the formation of dense GMCs, the young star clusters, the population of isolated massive stars, and also result in the present-day high star formation rate in the Galactic Centre.

An important side result of this paper is that the same feedback model appears to work for quasars as their SMBHs establish the $M - \sigma$ relation and clear the host galaxies of gas (e.g. King 2003, 2005; Nayakshin & Power 2010), as well as for a short burst of activity in Sgr A*, a SMBH that is somewhat below the $M - \sigma$ relation in a quiescent galaxy. This finding suggests that there is nothing fundamentally different between feedback from SMBHs at gas-rich epochs ($z \gtrsim 2$) and that from local galactic nuclei, except for the lower amount of fuel they receive.

More detailed future treatment of the feedback process, with improvements in both the physics of the simulations and more realistic observationally constrained initial conditions, may provide interesting and unique constraints on cosmological models of AGN feedback.

ACKNOWLEDGMENTS

This research used the ALICE High Performance Computing Facility at the University of Leicester. Some resources on ALICE form part of the DiRAC Facility jointly funded by STFC and the Large Facilities Capital Fund of BIS.

KZ is supported by an STFC studentship. Theoretical astrophysics research in Leicester is supported by an STFC Rolling Grant.

REFERENCES

- Alexander, R. D., Smedley, S. L., Nayakshin, S., & King, A. R. 2012, MNRAS, 419, 1970
- Baganoff, F. K., Maeda, Y., Morris, M., & et al. 2003, ApJ, 591, 891
- Bartko, H., et al. 2009, ApJ, 697, 1741
- Blandford, R., & Eichler, D. 1987, Phys.Rep., 154, 1
- Blandford, R. D., & Begelman, M. C. 1999, MNRAS, 303, L1
- Cheng, K.-S., Chernyshov, D. O., Dogiel, V. A., Ko, C.-M., & Ip, W.-H. 2011, ApJL, 731, L17+
- Ciotti, L., & Ostriker, J. P. 1997, ApJL, 487, L105+
- Crocker, R. M. 2011, ArXiv e-prints

- Crocker, R. M., & Aharonian, F. 2011, *Physical Review Letters*, 106, 101102
- Crocker, R. M., Jones, D. I., Aharonian, F., & et al. 2011, *MNRAS*, 413, 763
- Cuadra, J., Nayakshin, S., & Martins, F. 2008, *MNRAS*, 383, 458
- Dahmen, G., Huttemeister, S., Wilson, T. L., & Mauersberger, R. 1998, *A&A*, 331, 959
- Dame, T. M., Hartmann, D., & Thaddeus, P. 2001, *ApJ*, 547, 792
- Dobler, G., Cholis, I., & Weiner, N. 2011, *ApJ*, 741, 25
- Figer, D. F., Kim, S. S., Morris, M., Serabyn, E., Rich, R. M., & McLean, I. S. 1999a, *ApJ*, 525, 750
- Figer, D. F., McLean, I. S., & Morris, M. 1999b, *ApJ*, 514, 202
- Finkbeiner, D. P. 2004, *ApJ*, 614, 186
- Gammie, C. F. 2001, *ApJ*, 553, 174
- Ghez, A. M., Salim, S., Hornstein, S. D., & et al. 2005, *ApJ*, 620, 744
- Ghez, A. M., et al. 2008, *ApJ*, 689, 1044
- Goodman, J. 2003, *MNRAS*, 339, 937
- Goto, M., et al. 2008, *ApJ*, 688, 306
- Guesten, R., Genzel, R., Wright, M. C. H., Jaffe, D. T., Stutzki, J., & Harris, A. I. 1987, *ApJ*, 318, 124
- Guo, F., & Mathews, W. G. 2011, *ArXiv e-prints*
- Hobbs, A., & Nayakshin, S. 2009, *MNRAS*, 394, 191
- Hobbs, A., Nayakshin, S., Power, C., & King, A. 2011, *MNRAS*, 413, 2633
- Immer, K., Schuller, F., Omont, A., & Menten, K. M. 2012, *A&A*, 537, A121
- Jones, P. A., et al. 2011, *MNRAS*, 1895
- King, A. 2003, *ApJL*, 596, L27
- King, A. 2005, *ApJL*, 635, L121
- King, A. R. 2010a, *MNRAS*, 402, 1516
- King, A. R. 2010b, *MNRAS*, 408, L95
- King, A. R., Zubovas, K., & Power, C. 2011, *MNRAS*, L263+
- Kinney, A. L., Schmitt, H. R., Clarke, C. J., & et al. 2000, *ApJ*, 537, 152
- Mauerhan, J. C., Muno, M. P., Morris, M. R., Stolovy, S. R., & Cotera, A. 2010, *ApJ*, 710, 706
- McKee, C. F. 1990, in *Astronomical Society of the Pacific Conference Series*, Vol. 12, *The Evolution of the Interstellar Medium*, ed. L. Blitz, 3–29
- McKee, C. F., & Cowie, L. L. 1975, *ApJ*, 195, 715
- Mertsch, P., & Sarkar, S. 2011, *Physical Review Letters*, 107, 091101
- Molinari, S., Bally, J., Noriega-Crespo, A., & et al. 2011, *ApJL*, 735, L33+
- Morris, M., Ghez, A. M., & Becklin, E. E. 1999, *Advances in Space Research*, 23, 959
- Morris, M., & Serabyn, E. 1996, *ARA&A*, 34, 645
- Nagar, N. M., & Wilson, A. S. 1999, *ApJ*, 516, 97
- Narayan, R., Yi, I., & Mahadevan, R. 1995, *Nature*, 374, 623
- Nayakshin, S., Cha, S.-H., & Hobbs, A. 2009, *MNRAS*, 397, 1314
- Nayakshin, S., & Cuadra, J. 2005, *A&A*, 437, 437
- Nayakshin, S., Cuadra, J., & Springel, V. 2007, *MNRAS*, 379, 21
- Nayakshin, S., Dehnen, W., Cuadra, J., & Genzel, R. 2006, *MNRAS*, 366, 1410
- Nayakshin, S., & Power, C. 2010, *MNRAS*, 402, 789
- Nayakshin, S., Sazonov, S., & Sunyaev, R. 2012, *MNRAS*, 419, 1238
- Paumard, T., Genzel, R., Martins, F., & et al. 2006, *ApJ*, 643, 1011
- Pierce-Price, D., et al. 2000, *ApJL*, 545, L121
- Ponti, G., Terrier, R., Goldwurm, A., Belanger, G., & Trap, G. 2010, *ApJ*, 714, 732
- Pounds, K. A., & Vaughan, S. 2011, *MNRAS*, 415, 2379
- Reid, M. J., Menten, K. M., Zheng, X. W., Brunthaler, A., & Xu, Y. 2009, *ApJ*, 705, 1548
- Revnivtsev, M. G., Churazov, E. M., Sazonov, S. Y., & et al. 2004, *A&A*, 425, L49
- Rice, W. K. M., Lodato, G., & Armitage, P. J. 2005, *MNRAS*, 364, L56
- Sazonov, S. Y., Ostriker, J. P., & et al. 2005, *MNRAS*, 358, 168
- Schödel, R., Ott, T., Genzel, R., & et al. 2002, *Nature*, 419, 694
- Scoville, N. Z., Solomon, P. M., & Penzias, A. A. 1975, *ApJ*, 201, 352
- Serabyn, E., Shupe, D., & Figer, D. F. 1998, *Nature*, 394, 448
- Shakura, N. I., & Sunyaev, R. A. 1973, *A&A*, 24, 337
- Snowden, S. L., Egger, R., Freyberg, M. J., & et al. 1997, *ApJ*, 485, 125
- Sofue, Y. 2011, *ArXiv e-prints*
- Soltan, A. 1982, *MNRAS*, 200, 115
- Springel, V. 2005, *MNRAS*, 364, 1105
- Stolte, A., Ghez, A. M., Morris, M., Lu, J. R., Brandner, W., & Matthews, K. 2008, *ApJ*, 675, 1278
- Su, M., Slatyer, T. R., & Finkbeiner, D. P. 2010, *ApJ*, 724, 1044
- Sunyaev, R., & Churazov, E. 1998, *MNRAS*, 297, 1279
- Sutherland, R. S., & Dopita, M. A. 1993, *ApJS*, 88, 253
- Terrier, R., Ponti, G., Bélanger, G., & et al. 2010, *ApJ*, 719, 143
- Thompson, T. A., Quataert, E., & Murray, N. 2005, *ApJ*, 630, 167
- Tombesi, F., Cappi, M., Reeves, J. N., Palumbo, G. G. C., Yaqoob, T., Braitto, V., & Dadina, M. 2010a, *A&A*, 521, A57
- Tombesi, F., Sambruna, R. M., Reeves, J. N., Braitto, V., Ballo, L., Gofford, J., Cappi, M., & Mushotzky, R. F. 2010b, *ApJ*, 719, 700
- Toomre, A. 1964, *ApJ*, 139, 1217
- Yusef-Zadeh, F., et al. 2009, *ApJ*, 702, 178
- Zubovas, K., & King, A. 2012, *ApJL*, 745, L34
- Zubovas, K., King, A. R., & Nayakshin, S. 2011, *MNRAS*, 415, L21